(4)

AFAL-TR-88-031

AD:

DTIC FILE COPY

AD-A197 537

21st Century Propulsion Concept

Final Report
for the period
7 July 1987 to
7 January 1988

DTIC
ELECTE
AUG 1 9 1988
S D
CD

April 1988

Author:
R. L. Talley

Veritay Technology, Inc.
P. O. Box 305
4845 Millersport Highway
East Amherst, NY 14051

F04-88-1
F04611-87-C-0058

Approved for Public Release

Prepared for the: **Air Force Astronautics Laboratory**

Air Force Space Technology Center
Space Division, Air Force Systems Command
Edwards Air Force Base,
California 93523-5000

88 8 16

NOTICE

When U.S. Government drawings, specifications, or other data are used for any purpose other than a definitely related Government procurement operation, the fact that the Government may have formulated, furnished, or in any way supplied the said drawings, specifications, or other data, is not to be regarded by implication or otherwise, or in any way licensing the holder or any other person or corporation, or conveying any rights or permission to manufacture, use, or sell any patented invention that may be related thereto.

FOREWORD

This final report was submitted by Veritay Technology, Inc., East Amherst, NY on completion of Small Business Innovative Research contract F04611-87-C-0058 with the Air Force Astronautics Laboratory (AFAL), Edwards AFB, CA. AFAL Project Manager was Dr Frank Mead.

This report has been reviewed and is approved for release and distribution in accordance with the distribution statement on the cover and on the DD Form 1473.

Franklin B. Mead Jr.
FRANKLIN B. MEAD, JR.
Project Manager

William A. Sowell
WILLIAM A. SOWELL, CAPT, USAF
Chief, Advanced Concepts Branch

FOR THE COMMANDER

Robert L. Geisler
ROBERT L. GEISLER
Deputy Chief, Astronautical Sciences Division

UNCLASSIFIED
SECURITY CLASSIFICATION OF THIS PAGE

ADA197537

REPORT DOCUMENTATION PAGE

1a. REPORT SECURITY CLASSIFICATION UNCLASSIFIED	1b RESTRICTIVE MARKINGS
2a. SECURITY CLASSIFICATION AUTHORITY	3. DISTRIBUTION / AVAILABILITY OF REPORT Approved for public release, distribution is unlimited.
2b. DECLASSIFICATION / DOWNGRADING SCHEDULE	
4. PERFORMING ORGANIZATION REPORT NUMBER(S) F04-88-1	5. MONITORING ORGANIZATION REPORT NUMBER(S) AFAL-TR-88-031
6a. NAME OF PERFORMING ORGANIZATION Veritay Technology, Inc. 6b OFFICE SYMBOL (If applicable) 7V715	7a. NAME OF MONITORING ORGANIZATION Air Force Astronautics Laboratory
6c. ADDRESS (City, State, and ZIP Code) 4845 Millersport Highway, PO Box 305 East Amherst, New york 14051	7b. ADDRESS (City, State, and ZIP Code) LKCT Edwards AFB, CA 93523-5000
8a. NAME OF FUNDING / SPONSORING ORGANIZATION 8b OFFICE SYMBOL (If applicable)	9. PROCUREMENT INSTRUMENT IDENTIFICATION NUMBER F04611-87-C-0058
8c. ADDRESS (City, State, and ZIP Code)	10. SOURCE OF FUNDING NUMBERS PROGRAM ELEMENT NO. 65502F; PROJECT NO. 3058; TASK NO. 00; WORK UNIT ACCESSION NO. 4M

11. TITLE (Include Security Classification)
21st Century Propulsion Concept (U)

12. PERSONAL AUTHOR(S)
Talley, Robert L.

13a TYPE OF REPORT	13b. TIME COVERED	14. DATE OF REPORT (Year, Month, Day)	15. PAGE COUNT
Final	FROM 87/7/1 TO 88/1/7	88/4	73

16. SUPPLEMENTARY NOTATION

17 COSATI CODES			18. SUBJECT TERMS (Continue on reverse if necessary and identify by block number)
FIELD	GROUP	SUB-GROUP	
22	01		Biefield-Brown Effect; Electrostatic Force Generation; Electrostatic Field Propulsion; Payloads; Launching; Advanced Propulsion Techniques

19. ABSTRACT (Continue on reverse if necessary and identify by block number)

This Phase I SBIR contract effort was intended to explore the Biefield-Brown effect, which allegedly converts electrostatic energy into a propulsive force.

Activities under this program emphasized the experimental exploration of this electrostatic thrust-generation concept to verify its existence, to verify its operation in a vacuum, and to establish the magnitude of its thrust.

To meet these goals an overall laboratory test configuration was designed and developed for quantifying the electrostatically induced propulsive forces on selected experimental devices. This configuration utilized a vacuum chamber with a torsion fiber type measurement system for direct assessment of propulsive forces.

20 DISTRIBUTION / AVAILABILITY OF ABSTRACT ☐ UNCLASSIFIED/UNLIMITED ☒ SAME AS RPT. ☐ DTIC USERS	21. ABSTRACT SECURITY CLASSIFICATION Unclassified
22a NAME OF RESPONSIBLE INDIVIDUAL Franklin S. Mead, Jr.	22b TELEPHONE (Include Area Code) (805) 275-5540 22c. OFFICE SYMBOL

DD FORM 1473, 84 MAR 83 APR edition may be used until exhausted.
All other editions are obsolete

SECURITY CLASSIFICATION OF THIS PAGE

★U.S. Government Printing Office: 1985—639-012

19. ABSTRACT (CONT.)

Geometrical symmetries were incorporated in the design to minimize the influence of reaction forces which can arise from nearby bodies, including the walls of the vacuum chamber itself.

Tests were conducted at atmospheric pressure and over a range of partial vacuum conditions.

Direct experimental results indicate that when an electrostatic potential difference is applied between asymmetrical electrodes of an all metal test device, a residual propulsive force is generated and acts on the device. This residual force acts in the opposite direction to electrical wind forces and to the forces claimed to have been measured in a vacuum by T.T. Brown. Keywords:)

TABLE OF CONTENTS

Section	Page
INTRODUCTION	1
INVESTIGATIVE PROGRAM	3
LITERATURE SURVEY AND BACKGROUND	4
Literature Survey	4
Background and Review of Selected Observations	4
EXPERIMENTAL CONFIGURATION	9
General	9
Main Test Configuration	13
Torsion Fiber Subsystem	15
Optical Readout and Data Acquisition Subsystems	21
Electrical Subsystem	24
Vacuum Subsystem	27
Test Devices	29
TEST RESULTS	31
Test Approach	31
Calibration	32
Device Tests	35
Auxiliary Tests and Considerations	52
System Errors	53
Evaluation	54
CONCLUSIONS	58
RECOMMENDATIONS	61
REFERENCES	62
BIBLIOGRAPHY	64

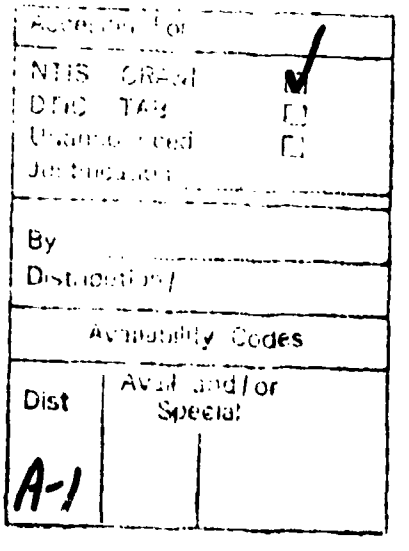

LIST OF FIGURES

Figure	Caption	Page
1	Block Diagram of Overall Test Layout	10
2	Room Layout	12
3	Test Configuration Schematic	14
4	Figure-Eight Device Support	16
5	Details of Rotating Device Support and Fixed Standpipe in Electrical Connection Region	26
6	Variation of Measured Force With Air Pressure	42
7	Variation of Measured Force With Applied Potential Difference	45
8	Variation of Measured Force With Applied Potential Difference	47

LIST OF TABLES

Table	Title	Page
1	Selected Mechanical Properties of Metal Fibers	17
2	Parameters for Calibration Cylinder and Mirror Holder	21
3	Brown Effect Test Device No. 1	30
4	Brown Effect Test Device No. 2	30
5	Cone for Brown Effect Test Device No. 3	30
6	Calibration: Torsion Fiber No. 1	33
7	Asymmetrical Devices Test Data Summary	38
8	Symmetrical Device Data Summary	49
9	Electrical Conditions for Symmetrical Device Tests	50
10	Array for Comparison of Forces Measured Using Symmetrical Device	51

INTRODUCTION

The objective of this contract effort was to experimentally and theoretically explore the Biefield-Brown effect, which allegedly converts electrostatic energy into a propulsive force.

This force-generation scheme, originally suggested by Dr. Paul Biefield and subsequently discovered by Townsend T. Brown in the late 1920s, arises when a large DC electrical potential difference is applied between shaped electrodes fixed with respect to one another by a dielectric. Under these conditions a significant net force is generated, which acts on the entire electrode/dielectric body and typically causes it to move in the direction of the positive electrode.

This concept may well represent a direct field-field, or field-vacuum interaction scheme with the potential for producing thrust without the conventional action-reaction type of momentum transfer brought about by ejective expenditure of an onboard fuel. The significance of this propulsion concept to launching and/or maneuvering payloads in space is potentially very great.

This concept has received cursory attention over a period of many years, but at the outset of the present effort it was still inadequately explored and remained without confirmed operation in a vacuum, without adequate quantitative characterization, and without an adequate theoretical basis for its operation.

Therefore, activities under the current program emphasized the experimental exploration of this electrostatic, thrust-generation concept to verify its very existence, to verify its operation in a vacuum and to establish the magnitude of its thrust. To conduct this program, an overall laboratory test design and configuration was developed that was suitable for quantifying the resultant propulsive force. Instrumentation schemes and techniques were also developed for measuring the

propulsive force and key physical parameters. Candidate propulsive devices were developed and tested. The overall experimental effort centered on making direct measurements of electrostatically induced propulsive forces on these test devices, inasmuch as details of the nature of the Brown effect were too sketchy to provide a reliable base for interpreting indirect measurements. Theoretical activities centered largely on examining contributions from known phenomena, which could influence or confound measured force values.

This report discusses the various features of the investigation, including a search and review of the available literature relevant to the Brown effect, the experimental configuration, the test techniques and results, the evaluations made, and the findings and recommendations to further explore and develop the potential of the Brown effect.

The experimental results of this investigation give a preliminary indication that a force phenomena does arise in conjunction with the presence of a non-linear electrostatic field. At present these findings are based on very limited results. Additional tests and efforts will be required to confirm or refute this finding. We are cautiously optimistic that this finding will remain valid when the results of other possible minor effects are explored and evaluated.

INVESTIGATIVE PROGRAM

An experimental-theoretical approach was used to explore the existence and nature of the Biefield-Brown effect. Particular attention was given to developing an experimental configuration and technique to provide a sound basis for quantifying electrostatically induced propulsive forces on selected test devices, and to overcome shortcomings of previous experiments that have led to criticism of Brown's work. This program was carried out in the following three phases:

1. Literature search and review---This included a search and review of the available literature related to the Biefield-Brown effect, its nature, and its use for propulsion.

2. Experimental evaluation---This involved developing an overall laboratory test design and configuration suitable for quantifying the propulsive force; advancing instrumentation schemes for measuring the propulsive force and relevent physical parameters; designing, fabricating and testing candidate propulsive devices; and evaluating the test results.

3. Theoretical studies---This primarily involved finding key parameters and recognized phenomena on which the Biefield-Brown effect may depend. Secondarily, considerations were given to developing a preliminary theoretical model for the propulsion concept, mainly for use in designing the experiments and evaluating the test results.

LITERATURE SURVEY AND BACKROUND

Literature Survey

Information directly related to the Biefield-Brown effect (sometimes just called the Brown effect) is rather limited, often obscure, and sometimes hard to acquire. A reasonable sample of past and current material written about the Brown effect has been acquired, or at least identified. A bibliography of these and other references believed to be relevant is presented later in this report.

It is noted that a portion of the most definitive work of T.T. Brown has been reported in the patent literature. Other published articles written directly by Brown are scarce. His findings and views have occasionally been summarized by others. The six-volume set entitled, "The Scientific Notebooks of T.T. Brown," (currently being published) is worthy of note, but information related to Brown's propulsion work seems to be limited to Volume 1 and part of Volume 2.

Background and Review of Selected Observations

The impetus for T.T. Brown to conduct electrostatic- type propulsion investigations apparently received a considerable boost from Dr. Biefield's query as to whether an electrical capacitor, hung by a thread, would have a tendency to move when it was given a heavy electrical charge. "Yes," was the answer found by Brown. This finding formed the essential basis for the Biefield-Brown effect.[1] Subsequently, Brown broadened the phenomenological basis of his investigations to consider possible couplings between the forces of electricity and gravity, as analogs to known couplings between those of electricity and magnetism. Whereas the coil is a key link in electromagnetic phenomena, the capacitor is the analogous link for the electrogravitational case. This, in turn, may account for

Brown's emphasis on the use of capacitor-type propulsion devices, including the use of dielectrics.

Five factors were indicated by Brown as determining the intensity of the effect:[2]

1. The separation of the plates of the capacitor (closer plates give a greater effect);

2. The magnitude of the dielectric constant K (larger K gives a greater effect);

3. The area of the capacitor plates (larger plates give a greater effect);

4. The potential difference applied to charge the plates (larger potential difference gives a larger effect); and

5. The mass of the dielectric between the plates (greater mass gives a larger effect).

Brown claimed that it was the last factor which is inexplicable from the electromagnetic viewpoint, and which provides the connection with gravity.

Essentially, the force produced in Brown's experiments was nearly always in the same direction as that from the negative to the positive potential within the test device. It is important to note, however, that in his early dielectric-type devices the force and motion sometimes would also occur in the reverse direction, when the so-called "saturation voltage" of the dielectric was exceeded.[3]

Later---when Brown used asymmetrical devices---apparently no ambiguity in the direction of the propulsion force was observed.

In these devices, a pair of different sized electrodes was attached to opposite ends of a dielectric element. When a high electrostatic potential difference was applied across these electrodes, the electric field lines from one electrode converged steeply to the other. The force tending to propel the device was, in this case, in a direction from the region of high flux density toward the region of low flux density, and generally in the direction through the axis of the electrodes.[4] Brown further claimed:[4]

> " The thrust produced by such a device is present if the electrostatic field gradient between the two electrodes is non-linear. This non-linearity of gradient may result from a difference in configuration of the electrodes, from the electrical potential and/or polarity of adjacent bodies, from the shape of the dielectric member, from a gradient in the density, electrical conductivity, electric permittivity and magnetic permeability of the dielectric member or a combination of these factors".

In another set of experiments,[5] Brown observed an impulse (or time-dependent) action with a type of test device made from a solid block of massive dielectric. Such a test device was immersed in oil, but suspended with electrical leads to act as a pendulum and swing along the line of its elements (i.e., lengthwise). When a DC potential in the range of 75 to 300 kilovolts was applied, the pendulum swung up the arc and stopped when the vertical component of the propulsive force balanced the gravitational force on the pendulum. But the pendulum did not remain there; it gradually returned to the starting position even while the potential was maintained. The time for the pendulum to reach the maximum amplitude of swing was less than five seconds, but from 30 to 80 seconds were required for it to return to zero. It was necessary to remove the electrical potential for several minutes to allow the system to regain its normal condition and to enable the cycle to be repeated.

The observations made by Brown can likely be accepted at face value, but his claims and explanations are another matter. Unfortunately, despite Brown's efforts to the contrary, his results and explanations have been repeatedly reviewed, evaluated, criticized and often discredited[6] with little attempt to adequately explore his observations---largely because the reviewers found it impossible to accept the possibility that the Biefield-Brown effect could represent a "new force."

Thus, at the outset of this program, the literature discussing Brown's work reported no confirmation of the existence of the effect in a vacuum, no adequate characterization of the effect in quantitative terms, and no theoretical basis for the observed generation of the effect.

From the space-propulsion point of view, the issue of operation in a vacuum is paramount. A known phenomenon called "electrical (or ion) wind"[7] has frequently been invoked as the mechanistic basis of thrust on electrostatic-driven propulsion devices similar to, and including, those explored by Brown. In fact, electrical wind does contribute to the thrust on such devices when they operate in air.* However, Brown[4] has made the claim:

> " In a vacuum, the reaction forces appear on solid environmental bodies, such as the walls of the vacuum chamber. The propelling force, however, is not reduced to zero when all environmental bodies are removed beyond the apparent range of the electrical field."

---

* The electrical or ion wind effect typically arises in the vicinity of coronas and results from the momentum given to air molecules by impact or drag of the ions and electrons as they move out from the high field regions.

Further, in a 1973 letter written to Rho Sigma,** Brown commented on his propulsion investigations in a vacuum environment:(2)

> " The experiments in a vacuum were conducted...in 1955-56...in 1957-58 and...in 1959....We were aware that the thrust on the electrode structures was caused largely by ambient ion momentum transfer when the experiments were conducted in air....In the Paris test miniature saucer-type airfoils were operated in a vacuum exceeding 10^{-6} mmHg. Bursts of thrust (towards the positive) were observed every time there was a vacuum spark within the bell jar....The result which was most significant from the standpoint of the Biefield-Brown effect was that thrust continued, <u>when there was no vacuum spark</u>, causing the rotor to accelerate in the negative to positive direction....In short, it appears there is strong evidence that the Biefield-Brown effect does exist in the negative to positive in a vacuum of at least 10^{-6} Torr. The residual thrust is several orders of magnitude larger than the remaining ambient ionization can account for."

Thus, we focused the activities of the current program on experimentally determining the existence or nonexistence of the phenomenon, confirming its operation in a vacuum, and establishing the magnitude of its thrust in quantitative terms. The following section describes the experimental configuration designed and built by Veritay for this purpose.

** Rho Sigma is a pseudonym

EXPERIMENTAL CONFIGURATION

General

A principal step in investigating the Biefield-Brown effect is the development of a test configuration for quantifying this electrostatically induced propulsive force on candidate propulsion devices. The configuration design advanced and implemented for this project uses a vacuum chamber as the central element. This permits tests to be conducted either at atmospheric pressure or over a range of partial vacuum conditions. Further, the test set-up incorporates geometrical symmetries to minimize the influence of reaction forces, which may arise from nearby bodies, including the walls of the vacuum chamber itself.

These features reflect the importance of investigating the Brown effect over a range of pressure conditions, and especially in a vacuum. Under normal atmospheric conditions, electrical wind effects are known to be significant, and can be sufficient to account for some of the results often attributed to the Brown effect.

A block diagram of the overall test layout is given in Figure 1. This figure shows schematically the key components, their grouping into functional subsystems, and their interconnections within the subsystems.

The subsystems include the following:

1. Main test configuration, which encompasses the vacuum chamber and the components within its interior.

2. Torsion fiber subsystem, which is the central element for measuring propulsive forces, is located

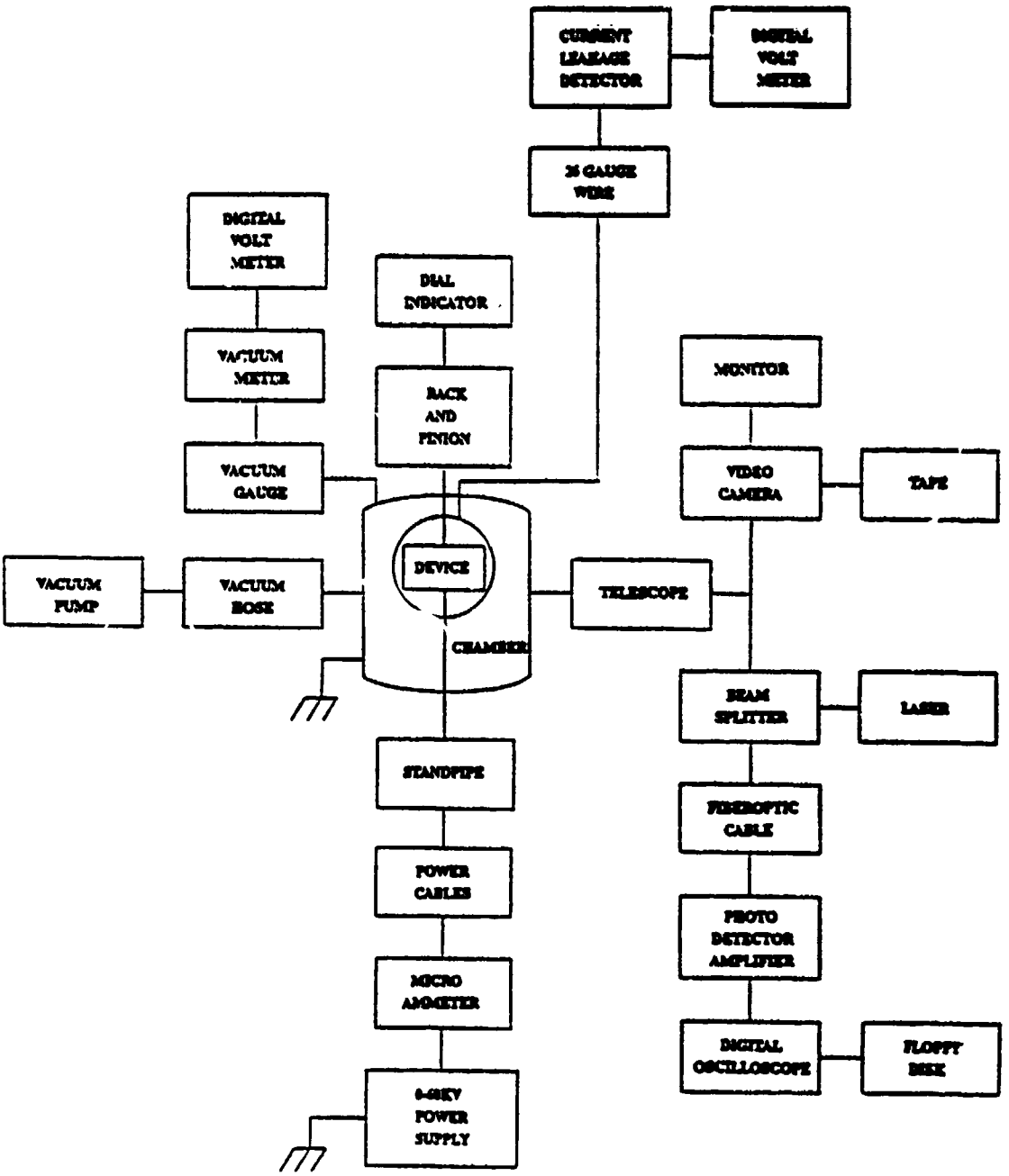

Figure 1. Block Diagram Of Overall Test Layout

inside the chamber, and is noted specifically because of its importance.

3. Optical readout and data acquisition subsystem, which is critical in extracting and recording measurement information. It interfaces with the chamber through the telescope.

4. Electrical subsystem, which includes both the high voltage source to activate the test devices and the instrumentation to quantify several electrical quantities.

5. Vacuum subsystem, which includes the pump, gauges and components related to achieving and quantifying partial vacuum conditions in the chamber.

6. Test devices, which are critical to meaningful exploration of the Brown effect.

The actual implementation of this test layout, shown by the physical arrangement of various components, is given in the room layout of Figure 2. The room itself is located in the corner of a concrete bunker, formerly a part of the Nike missile launch site. The concrete floor is approximately 4.8 m (16 feet) below grade, and the concrete ceiling is covered with about 1 m (3 feet) of earth and another 0.2 m (8 inches) of concrete at the surface. The short-term temperature stability of this room location is good without imposing controls, and the mechanical vibration stability during test runs is adequate to maintain a low mechanical noise level in the experimental measurements.

Details of these experimental features are discussed in subsequent subsections.

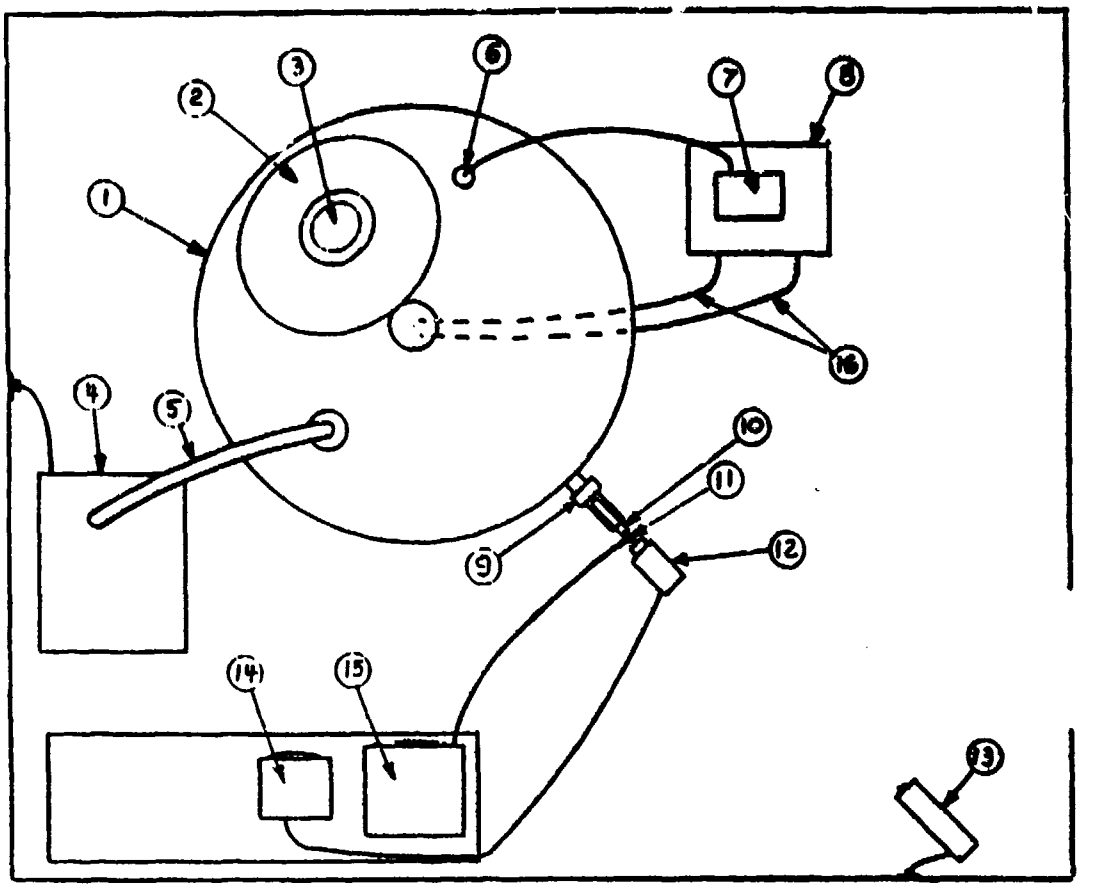

1.	VACUUM CHAMBER	9.	OBSERVATION PORT
2.	MANWAY COVER	10.	TELESCOPE
3.	ILLUMINATION PORT	11.	BEAM SPLITTER
4.	VACUUM PUMP	12.	VIDEO CAMERA
5.	VACUUM HOSE	13.	LASER
6.	VACUUM GAUGE	14.	MONITOR
7.	VACUUM METER	15.	OSCILLOSCOPE
8.	POWER SUPPLY	16.	POWER CABLES

Figure 2. Room Layout

Main Test Configuration

The main test configuration is shown schematically in Figure 3. It consists of an AISI type 316 stainless steel vacuum chamber approximately 1.04 m (40.8 inches) in diameter by 1.52 m (60 inches) overall height with a 1.17 m (46 inches) straight side and a welded, dished top and bottom. Access to the chamber is provided through a 0.51 m (20 inch) top manway and smaller ports. The latter are used as instrumentation, illumination and vacuum ports. The chamber is mounted on legs (not shown) with leveling screws for adjustment of the vertical axis of the chamber.

Other general features associated with the test configuration are also indicated in Figure 3. Candidate devices for the Brown effect tests are mounted in tandem on a figure-eight type device support. This unit with an attached mirror is suspended from the top of the chamber by a torsion fiber. The latter is fastened to a vacuum-sealed adjustable rod which can be raised, lowered or rotated, to achieve a suitable device height or angular zero position for tests.

The height adjustment for the fiber support rod was implemented by mounting the rod on a precision rack and pinion slide mechanism. In use, this unit was coupled with a dial indicator, and height settings and resettings to a precision of $\pm$ 0.0013 cm ($\pm$ 0.0005 inches) were achievable. This precision adjustment feature proved to be very important to the successful conduct of tests under this program.

The electrical input to the test devices are fed from a high voltage DC power supply into the bottom of the chamber through a standpipe, and are connected to concentric liquid mercury contacts at the top of the standpipe. Electricity is then fed to the test devices via conductors with points which touch the mercury. This arrangement provides nearly frictionless

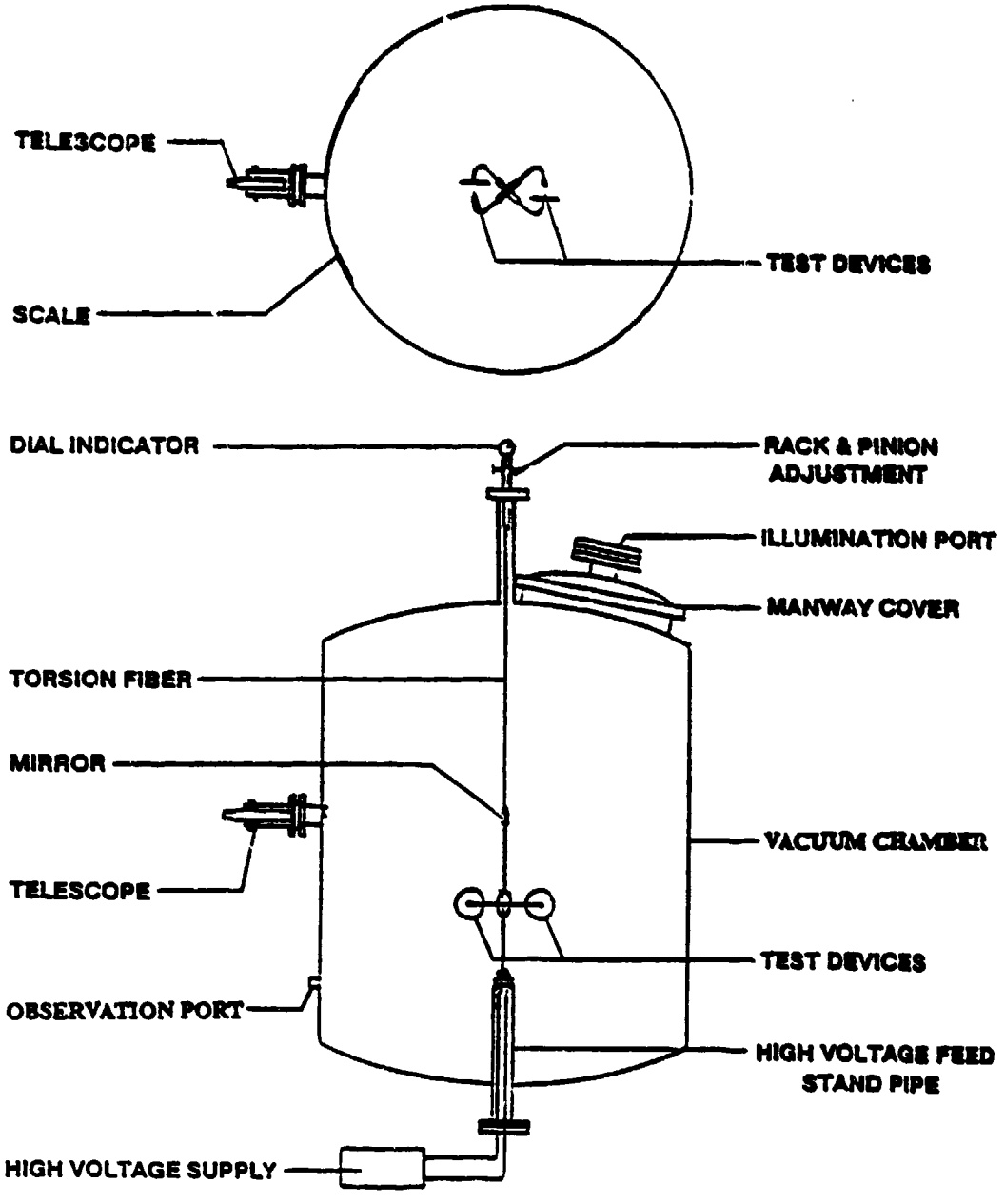

Figure 3. Test Configuration Schematic

electrical contacts, and permits electricity to be conducted to the test devices while a force measurement is being made.

A force measurement consists of determining the angular twist of the fiber caused by action of the force. This together with the fiber calibration constant and moment arms of the test devices permits the force acting on the devices to be evaluated. The angular twist of the torsion fiber during a test run is measured using a telescope, a mirror mounted to the test device support, and a scale fastened to the chamber wall.

Torsion Fiber Subsystem

The measurement of forces generated by electrostatically driven test devices is carried out using a single torsion fiber system which supports the devices. The torque to twist the fiber is provided by device generated forces which are directed perpendicularly to radial moment arms and to the fiber axis. Two such devices are directed in tandem and mounted on the figure-eight device support at "equal" radial distances from the fiber. The figure-eight device support is shown in Figure 4. The actual moment arm distances for tests conducted in this program were 0.1024 m and 0.1018 m, with an average value of 0.1021 m.

The selection of a torsion fiber involved making a tradeoff among a number of factors such as:

- elastic after-effect and hysteresis
- relative strength in tension and torsion
- elastic behavior almost up to the breaking point
- non-corrosive
- electrical insulators or conductors
- freedom from internal strains which can cause zero drift
- cost and availability.

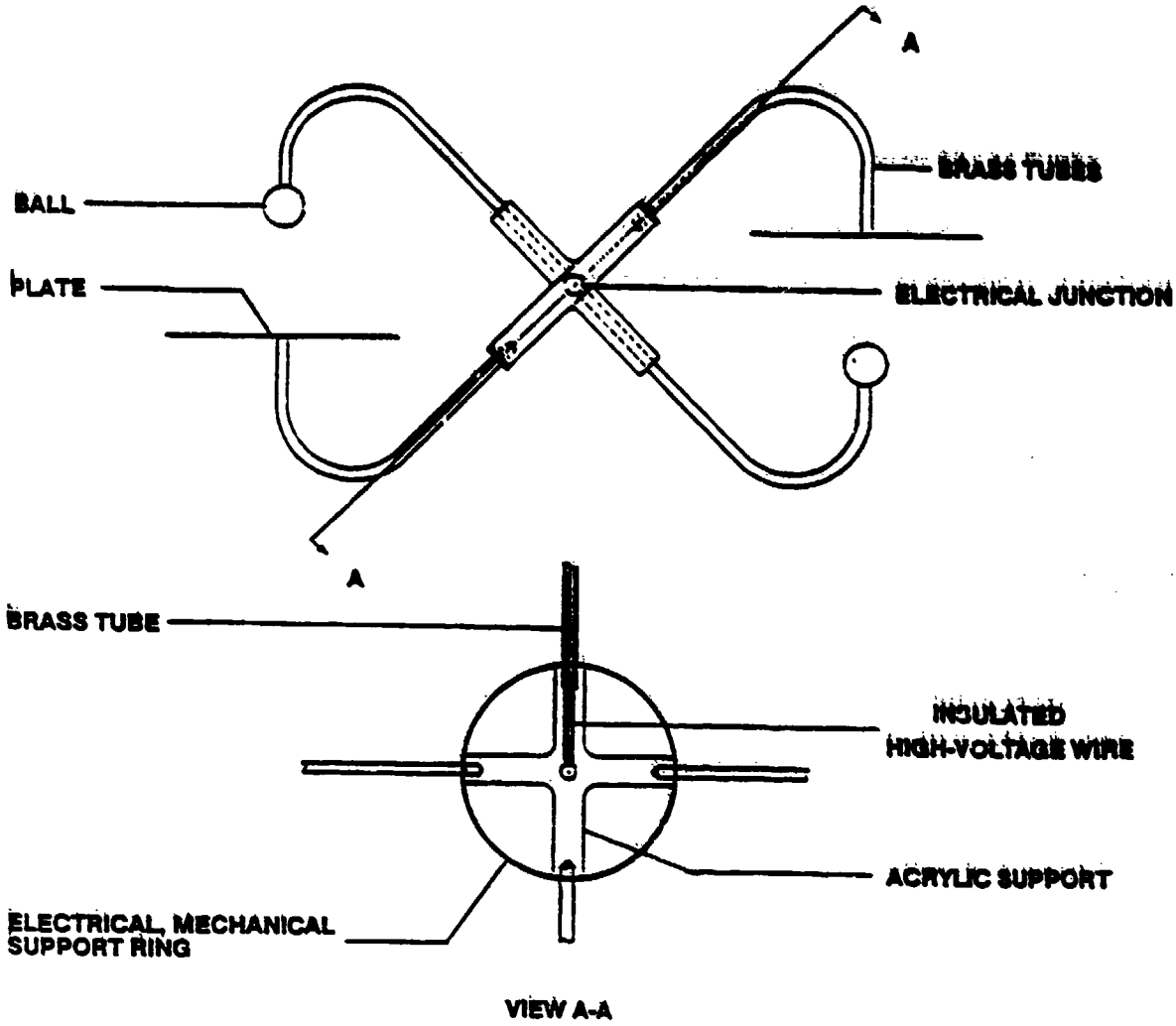

Figure 4. Figure-Eight Device Support

Metal fibers were of particular interest because of their electrical conductivity. A conducting fiber was expected to be used as an electrical lead for measuring the leakage current of various test devices; these tests have not yet been conducted. Metal fibers, however, are known to have long term drift problems. In this application we planned to make zero angular position readings of the fiber system both before, and after, each individual test, although zero drift was not expected to be a problem. In retrospect, drift has been observed occasionally, but has not been a serious problem. The drift observed was always linear over a period greater than the duration of a test and showed an average magnitude of about 1.7×10^{-4} radians per minute when it occurred. The drift continued at the same value when power was applied during a test run; deflections were measured directly between drift lines.

The types of metal fibers considered for use were copper, tungsten, platinum and silver. Selected mechanical properties of these fibers are given in Table 1.[8][9] Typically, the fiber strength becomes the limiting mechanical factor for each material and determines the corresponding minimum fiber diameter.

TABLE 1. Selected Mechanical Properties of Metal Fibers

MATERIAL	YOUNGS MODULUS $E(N/m^2)$	RIGIDITY MODULUS $G(N/m^2)$	TENSION YIELD N/m^2(psi)	DENSITY g/cm^3
Copper (hard)	$12.1\text{-}12.8\times10^{10}$	4.6×10^{10}	$5.24\times10^{8}(76\times10^{3})$	8.3-8.93
Tungsten	$34.\times 10^{10}$	13.5×10^{10}	$6.89\times10^{8}(100\times10^{3})$	18.6-19.1
Platinum (hard)	16.7×10^{10}	6.4×10^{10}	$4.14\times10^{8}(60\times10^{3})$	21.4
Silver (hard)	7.5×10^{10}	2.7×10^{10}	$3.58\times10^{8}(52\times10^{3})$	10.4

For reasons of availability and cost, together with features of strength, corrosion resistance and conductivity, the fiber type selected for test use was tin plated copper. Copper without the tin plating was sought, but was not readily available. The size of fiber used is B. and S. No.34 with a diameter of 160μm (0.0063 inches). This will support a load of 0.538 kg with a safety factor of two. The fiber length used is 0.927 m (36.5 inches).

Force measurement with a single torsion fiber system depends fundamentally on how the fiber twists when it is subjected to a torque. The total torque Q needed to twist a torsion fiber is given as the sum of three contributions[10]:

$$Q = Q_s + Q_z + Q_b \qquad (1)$$

where

Q_s = torque associated with the shear stress of twist (this torque constitutes the major part of the resistance of an elastic fiber to torsion)

Q_z = torque associated with the longitudinal stresses of twist (when an elastic member is twisted, its longitudinal fibers are forced to take up a helical configuration around the axis of the twist. The ones farthest from the axis are stretched and put in tension; this causes those near the axis to be put into compression).

Q_b = torque associated with the application of an axial force. (Since the tensile stress acts along helices, the force on each elementary area of the elastic member cross section has a component at right angles to the axis of twist. This component produces a torque dQ_b tending to untwist the member).

This can be written

$$Q = Q_s(1+Q_z/Q_s + Q_b/Q_s)$$

and for solid circular cross sections:

$$Q = Q_s \left(1 + 0.2\, q^2/G^2 + p/G \right) \qquad (2)$$

where

p = longitudinal tensile or compressive stress due to applied axial force

q = maximum shear stress of twist

G = shear (or torsion) modulus, also called modulus of rigidity.

In practice the ratio q/G is approximately .001 when the shear stress has its maximum allowable value. Q_z is therefore negligibly small compared to Q_s for typical amounts of twist. The quantity Q_b/Q_s or p/G is not negligible when heavy fiber loads are used.

The shear torque Q_s for this case is given by [10]

$$Q_s = (A^2 G\theta)/(2\pi L), \qquad (3)$$

with A= fiber cross sectional area
L= fiber length
θ= angle of twist in torsion connection.

Likewise, the torque Q_b is given by

$$Q_b = (PA\theta)/(2\pi L) \qquad (4)$$

with P= axial tensile (+) (or compressive (-)) force applied to a torsion connection (and hence to stretch a twisted fiber in tension).

These tension relations are included for completeness, and

are useful in the selection of fiber materials, and in evaluating the rigidity modulus G of materials.

Direct calibration of the torsion fiber used for tests was done by measuring the swing periods of the fiber as part of a torsional pendulum. In this case the torsional stiffness S of a fiber is given by [10]

$$S = Q/\theta = (4\pi^2 I_c)/T^2 \qquad (5)$$

where Q = total torque;N-m
θ = angle of twist of a torsion fiber;radians
I_c = moment of inertia of the suspended mass;kg-m^2
T = oscillation period;sec.

The connection between the torsional stiffness, S, and the rigidity modulus follows from equations (3) and (5),

$$G = S\ (2\pi L)/A^2\ . \qquad (6)$$

The fiber calibration is most conveniently carried out using a cylindrical block of known mass and dimensions, for which the moment of inertia can be determined with considerable accuracy.

A particularly important consideration noted nearly a century ago by Limb [11] concerns the shape of the oscillating calibration mass to be suspended from the torsion fiber under test. He noted that a solid cylinder with the length ℓ, which is $\sqrt{3}$ times its radius R, i.e. $\ell = R\sqrt{3}$, has the same momant of inertia about all axes through its centroid (the ellipsoid of inertia for the cylinder becomes a sphere). Therefore, by using a suspended mass of this shape for calibration, an error is not introduced if the point of attachment of the fiber to the cylinder does not lie exactly on the axis of the cylinder.

Such a calibration mass was employed, but the overall shape criterion was only approximately satisfied, since the contribution of the mass and moment of inertia of the mirror holder used to attach the calibration mass to the fiber were neglected. Values of key parameters for the calibration cylinder and mirror holder are given in Table 2.

TABLE 2.
Parameters For Calibration Cylinder and Mirror Holder

	CYLINDER	MIRROR HOLDER	TOTAL
Length, m(inch)	.02730(1.075)	----------	----------
Diameter, m(inch)	.03152(1.241)	----------	----------
Mass, kg	.16768	.01904	.18672
Moment of inertia, kg-m^2	2.1012×10^{-5}	3.3528×10^{-7}	2.1347×10^{-5}

Optical Readout and Data Acquisition Subsystems

A readout subsystem consisting of a simple telescope, mirror and scale was used to determine the angular twist of the torsion fiber. In this subsystem an alignment telescope equipped with a crosshair reticle is directed so its line of sight intersects, near center, a mirror attached to the lower end of the torsion fiber. The telescope and mirror are further positioned so this line of sight, after reflection, continues and intersects a linear scale fastened to the inner wall of the vacuum tank. The scale is mounted horizontally and is curved to conform to the shape of the wall.

The scale can then be viewed through the telescope and a definite reading determined at the intersection of the crosshair with the scale image. A change in the angular direction θ of the mirror causes a deflection of the light path through an angle 2θ. Concurrently, this causes an apparent movement of the scale image relative to the crosshair. For a scale deflection $(x-x_o)$, relative to some zero reading x_o, the angular motion of the mirror is $\theta = (x-x_o)/2r$.

In the arrangement used, the radial distance, r, from the mirror to the scale is 0.5175 m (20.38 inches). The scale, itself, is a stainless steel, flexible machinist's scale, 0.6096 m (24 inches) long with subdivisions in English units of 1/50 and 1/100 inches on two separate rulings.

The scale is typically read to the nearest 1.27×10^{-4} m (0.005 inches), and deflections of about twice this value are representative of the threshhold of measurement, taking into account reading uncertainties and random pendulum oscillations due to noise. This results in a minimum deflection angle of the mirror

$\theta_{min} = 2.45 \times 10^{-4}$ radian per 0.010 in. apparent motion of the scale.

This value of θ_{min} corresponds to about 50 seconds of arc, which is not of great sensitivity, but has proven to be a useful level for tests conducted under this program.

During propulsion device tests some observations were made visually through the telescope. A preferred technique involved using a video camera and monitor, with the camera lens positioned to see through the telescope eyepiece. Deflection readings during tests were then made directly from the video monitor and entered in a laboratory notebook manually.

A General Electric VHS movie Video System SE 9-9608 with video tape recorder was used for a number of the test runs. Use of the recorder permitted a real time record of the actual test run to be made. This record is helpful since it permits replaying the test run to confirm certain deflection readings or ascertain missing readings after-the-fact.

Readout of the torsion pendulum oscillations for calibration purposes required a different approach, since the swing time periods cannot be determined visually with sufficient accuracy. The same telescope and mirror system is again used, but an active signal in the form of a laser beam is passed through a beam-splitter, through the telescope, and onto the mirror. Twice each period as the mirror oscillates, the laser beam is reflected back through the telescope, into the beam splitter and deflected into a fiber optic cable and then onto a photodetector and amplifier. Real time electrical signals from the detector-amplifier are sent to a digital oscilloscope and recorder, where the signal pulse can be displayed and timed accurately.

For calibration runs, the zero angular position of the torsion fiber and mirror was adjusted so the laser beam was reflected into the detector when the pendulum passed its equilibrium position. Near this position the angular deflection rate of the mirror is the greatest, and the duration of the optical pulse at the photodetector will be close to a minimum. This facilitates making accurate measurements of the instant when the pulse occurs (usually reckoned at the maximum amplitude of the pulse).

The actual system assembled uses a Spectra Physics type 155A, 0.5 mW, helium-neon laser; a 10 mm x 10 mm prism beam splitter; a plastic fiber optic light guide; a photodiode detector with an IC instrumentation amplifier designed and built at Veritay; and a Nicolet Digital Oscilloscope Model 2090 with disk recorder.

Typical digital sampling times used were 0.05 seconds per point. At this sampling rate a total sample of 32 x 10^3 points (26.7 minutes) could be recorded directly. The total time used for calibration runs normally encompassed about six to eight complete oscillation periods.

This same data recording system employed for oscillation timing was also used to track early pump down runs in the vacuum chamber. In these vacuum checks, gauge readings were taken every 20 seconds, which provided a continuous 4000 point record that spanned approximately 22 hours.

Electrical Subsystem

High voltage was supplied to the devices under test with a Spellman regulated, 0-60 kV, DC power supply Model UHR60PN30, which has a maximum power output of 30 Watts. The voltage polarity of this supply can be reversed internally, but is not directly switchable for safety reasons.

The output voltage and current from this supply can be read directly on a panel mounted kilovoltmeter and microammeter, respectively. At low voltages and currents the sensitivity of these meters is inadequate. Input voltages up to about 2 kV were measured with a Fluke digital voltmeter model 77. A $\pm$ 5 A full scale instrument to measure supply current was designed and fabricated at Veritay. It consists of a high grade differential amplifier with programmable gain to accuratly measure the voltage drop across a precision resistor of known value. This unit has a minimum current resolution of about 100 A.

The high voltage is fed to the test devices inside the test chamber using Belden No. 8866-80C high voltage cables, which have a DC breakdown voltage of approximately 80 kilovolts. These cables penetrate, and are sealed with a high vacuum leak sealant,

to an acrylic plug at the base of the feed-through standpipe. The cables, themselves, are enclosed inside additional acrylic tubes inside the standpipe to help keep the cables straight and away from the grounded stainless steel walls of the standpipe. The conductors of these cables are attached to platinum wires at the top of the standpipe. These wires are sealed into the insulating acrylic block located there. This dielectric block, itself, is threaded into the interior of the standpipe and vacuum sealed to it with an O-ring and vacuum grease. The platinum wires then pass through this block to a shallow trough and well, each of which contains liquid mercury. The separated mercury regions are symmetric about the axis of the standpipe. Details of the electrical conductor location at the top of the standpipe are shown in Figure 5.

When the mercury is touched by conducting platinum points protruding from the base of the figure-eight device support, nearly frictionless electrical contacts are formed. These contacts permit the supply voltage to be fed directly to the test devices.

The standpipe column and dielectric block at its top were originally designed with provision to cool the liquid mercury. This was deemed necessary, since the liquid mercury was to be subjected to the full vacuum in the chamber, and mercury will boil at room temperature (20°C) under a vacuum of 0.160 Pascal (1.2×10^{-3} torr).[12] At a temperature of -5.6°C the vapor pressure of mercury is 1.33×10^{-2} P_a (10^{-4} torr), which is the lower limit which could be expected with the vacuum system used. These concerns were legitimate, but unfulfilled as other vacuum sealing problems (believed to be largely associated with the standpipe) precluded achieving vacuum levels in this system lower than about 1.3 Pascal (10^{-2} torr). Efforts to cool the mercury during this program were thus abandoned.

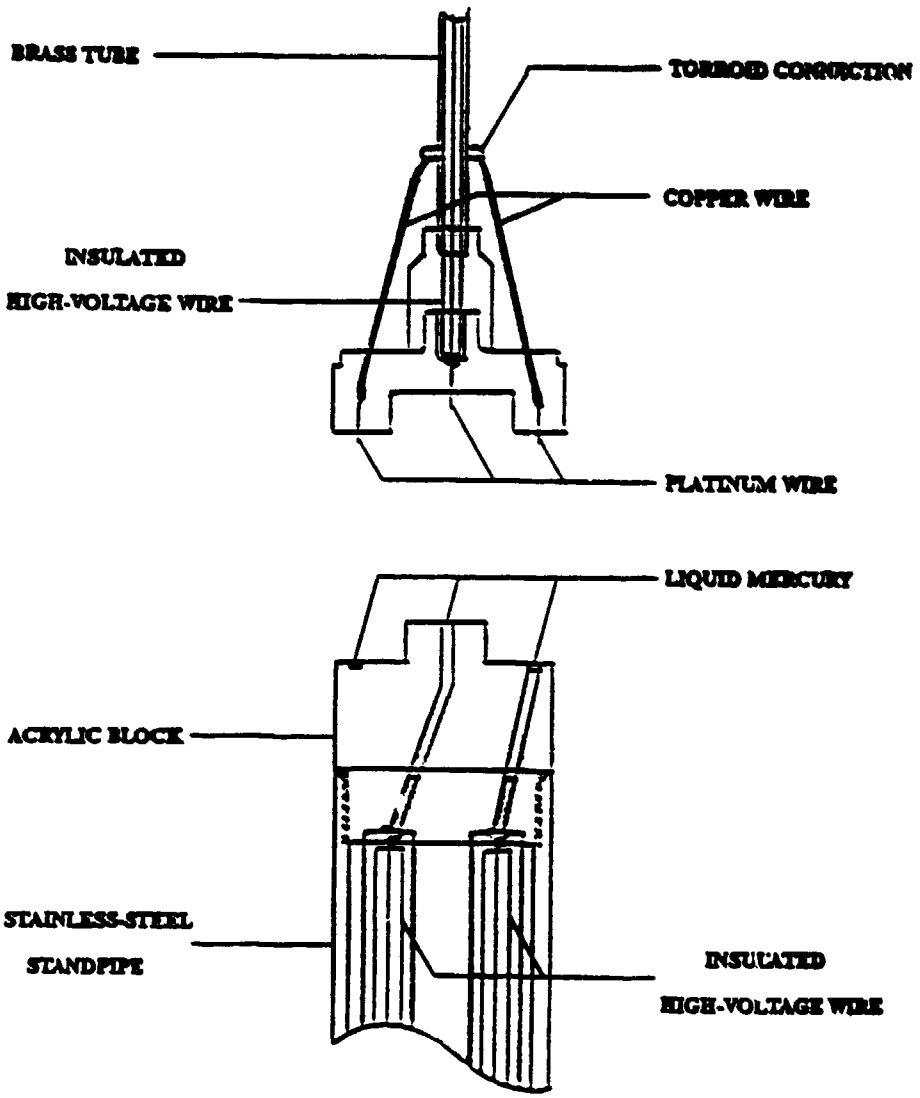

Figure 5. Details of Rotating Device Support And Fixed Standpipe in Electrical Connection Region

The surface tension and viscosity of the mercury did present problems of causing excessive friction for the contact points protruding from the device support. This was resolved by adjusting the fiber height so the contact points just touched the surface of the liquid mercury.

As part of the electrical considerations, an instrument for measuring the leakage current from the test devices was also developed. This leakage current meter is similar to the output current meter noted earlier, except this unit has four ranges of operation with the most sensitive being 0 to 500 nA. In this case the minimum resolution is 1 nA.

The collector for the leakage (diffusion) current from the test devices was a .406 m (16 inch) diameter stationary, hollow aluminum sphere, mounted inside and electrically insulated from the externally grounded vacuum tank, except via its connection through the leakage current instrument. This hollow sphere surrounded the figure-eight device support and test devices; the devices were free to rotate inside the sphere without contacting it.

In principal, the entire vacuum chamber could have been used as the leakage current detector. This would have involved isolating the entire chamber and associated equipment from electrical earth ground, and then connecting the chamber to earth ground through the leakage current meter. For safety reasons the chamber was not isolated from earth ground in this manner during the program.

Vacuum Subsystem

The vacuum achieved for test purposes was developed with a Boekel Cenco HYVAC 45, two stage rotary gear pump with gas ballast and 500 liter-per-minute (17.7 CFM) capacity. The vacuum

capability of this pump is 1.3 x 10^{-2} P_a(10^{-4} torr). While a lower vacuum level would have been desireable, the chamber size involved, the range of partial vacuum levels desired for test, the initial uncertainty as to the vacuum level needed to overcome electric wind effects, and pump costs precluded employing a pumping system in this program to achieve lower vacuum levels.

A Boeko TKO-19 vacuum pump fluid with a vapor pressure of 1.3 x 10^{-4} P_a (10^{-6} torr) at 25°C was used in the pump.

The pump was connected to the chamber with a reinforced, flexible vacuum hose with capability of holding a vacuum of about 1.3x10^{-4} P_a (10^{-6} torr).

All new flexible seals for the vacuum chamber ports were used, together with Dow Corning 976 vacuum grease and a high vacuum aerosol leak sealant, as required.

An Edwards Pirani gauge head PRM 10K with a model 503 controller was used as the primary means for routinely determining vacuum levels in this chamber. This controller unit has both a direct meter as well as an analog voltage signal for readout. This voltage signal was typically read out using a Fluke model 77 digital multimeter.

A Labconco McLeod gauge was available for calibration checks of the Pirani instrument.

Although strictly not a part of the vacuum system, an air inlet unit was installed on the vacuum tank. This unit consisted of Union Carbide type 4A molecular sieve dessicant and an EPM 2000 high volume air sampling filter to trap incoming aerosol particles larger than about 0.3 μm. Full utilization of this unit was not possible, since many of the test preparations required complete entry into the chamber.

Test Devices

The candidate devices selected for initial propulsion tests had all metal, but few or no dielectric components. This avoided the inherent problems associated with assessing initial and final electrical conditions when testing dielectrics [13] [14] and improved both the reproducibility and interpretability of results from a small number of tests.

One simple candidate device, which is patterned after a test device used by Brown [4], is the all metal ball and disk unit shown in Figure 4. The construction materials and device dimensions are given in Table 3. A key feature of this test unit is that it will develop a non-linear electric field gradient between the ball and disk.

A second test device is a pair of identical metal toroids, each with a flat disk which fills in the normally open central region of the toroid. The construction materials and dimensions of this device are given in Table 4. This test device is expected to develop a relatively uniform field between the two toroids.

Test device No. 3 was a modification of device No. 1, in which a truncated cone of dielectric was placed between the ball and disk. The material and cone dimensions are given in Table 5. Device No. 3 is expected to form a non-linear electric field gradient within the dielectric.

TABLE 3. Brown Effect Test Device No.1

Configuration: Ball and disk, separated normal to disk by 0.0400 m (1.57 inch)

	MATERIAL	DIAMETER	THICKNESS
Ball:	Aluminum	0.0127 m(0.50 inch)	-------
Disk:	Brass	0.0793 m(3.125 inch)	.00038 m (0.015inch)

TABLE 4. Brown Effect Test Device No.2

Configuration: Two filled in metal toroids coaxially located and separated by 0.0338m (1.33 inch).

	MATERIAL	DIAMETER		WEB THICKNESS
		OUTSIDE	INSIDE	
Toroid	Aluminum	.01905m (0.748inch)	.01270m (0.500inch)	.00122m (0.0048inch)

TABLE 5. Cone for Brown Effect Test Device No. 3

Configuration: Truncated dielectric cone to fit between the ball and disk of device No. 1.

	MATERIAL	DIAMETER		HEIGHT
		BASE	TOP	
Truncated Cone	Acrylic	0.0508m (2.000inch)	0.014m (0.55inch)	0.0455m (1.790inch)

TEST RESULTS

Test Approach

The overall test approach used here is directed toward measuring the propulsive forces over a range of partial vacuum conditions, and extrapolating these measures to a limit appropriate for a full vacuum. The purpose of this scheme, of course, is to overcome any residual force effects due to electrical wind. The propulsive force limit so obtained represents the sum of the Brown effect and the ion propulsion effect. The contribution due to ion propulsion can be estimated and the existence and magnitude of the Brown effect can be evaluated.

At the outset it was anticipated that separate, moveable walls might need to be installed in the chamber, and then tests run with the walls located at various distances from the devices to enable estimates to be made of the influence on the test devices of induced surface charge on the walls. Preliminary tests with boundary plates and devices outside the chamber led us to believe that such boundary effects were probably negligible, except perhaps at test conditions in excess of 20 kilovolts. Subsequent test results obtained in the chamber appear to confirm this expectation for the torsion fiber system, at least at relatively low voltage test conditions.

As noted earlier, a stationary hollow aluminum sphere (two joined hemispheres) was placed around the test device support as a collector for leakage currents from the associated devices. In effect, this sphere acted as a separate wall of the type just noted. The ability to neglect its influence as a boundary is important, in order to enable it to be used as a current collector.

Calibration

The calibration of torsion fibers was carried out by measuring the period of a torsion pendulum, consisting of the fiber, calibration cylinder and mirror holder.

Results for a first fiber are given in Table 6 over a range of vacuum levels. The torsional stiffness, S, of the fiber was calculated using equation (5) given previously. A regression analysis of the torsional stiffness as a function of vacuum level indicated essentially no change over the range of conditions tested. Thus a simple mean value of the torsional stiffness S was used. The corresponding rigidity modulus was calculated using equation (6); this gave a mean value $G=4.737 \times 10^{10} N/m^2$. This compares favorably with the handbook value $G_H = 4.6 \times 10^{10}$ N/m^2 for rolled copper. This first fiber was used for propulsion device shakedown test run numbers 1 through 8A, before it was accidentally broken while replacing a test device.

Thus a second similar wire, called fiber No.2, was calibrated at one atmosphere and at a temperature of $15.2^{o}C(59.4^{o}F)$. The value obtained for the torsional stiffness was $S= 3.2033 \times 10^{-6}$ $N-m^2$, and a corresponding value for the rigidity modulus was $G= 4.599 \times 10^{10}$ N/m^2. Fiber No.2 was used for propulsion device test runs after No. 8A, starting with No.9.

The effect of temperature on the fiber calibration values has not been measured directly, but was determined indirectly from data on the temperature variation of Youngs modulus for copper given by McGregor Tegart. [15] At $20^{o}C$ ($68^{o}F$) this coefficient is approximately -0.040 percent per degree Celsius increase ($-0.022\%/^{o}F$). This same coefficient applies approximately to the rigidity modulus, G, and to the torsional stiffness, S, of the copper fiber used. The small value of this coefficient indicates that temperature variations of

TABLE 6. Calibration: Torsion Fiber No.1

Fiber:

B&S:	No. 34 Tinned Copper
Diameter, D:	0.0160×10^{-2} m (0.0063 inch)
Length, L:	92.71×10^{-2} m (36.5 inch)
Cross Section Area, A:	2.014×10^{-8} m^2 (3.122×10^{-5} in^2)

Total Pendulum:

Mass, M_c	0.18672 kg
Moment, I_c	2.1347×10^{-5} kg-m^2

Data:

Test No.:	1C	2C	3C	4C	5C
No. of periods:	7	7	7	7	8
Temp, ^oC(^oF)	16.9 (62.4)	16.8 (62.2)	16.8 (62.2)	16.8 (62.2)	16.7 (62.0)
Vacuum, Pa(Torr	1.3 (10^{-2})	1.3 (10^{-2})	13.3 (10^{-1})	133 (1.0)	1330. (10.)
Swing period, sec.	15.974	15.987	15.982	15.986	15.982
± 1 sec	.0124	.0039	.0049	.0134	.0038
± 1 (%)	.078	.025	.031	.084	.024
Torsional Stiff. (S), N-m^2	3.3027×10^{-6}	3.2973×10^{-6}	3.2994×10^{-6}	3.2977×10^{-6}	3.2994×10^{-6}

Mean S, N-m^2	3.29931×10^{-6}
Mean Rigidity Modulus (G), N/m^2	4.737×10^{10}

± 2.4°C (± 4.3°F) experienced during the tests conducted under this program should alter the fiber calibration and resulting force values measured by no more than about ± 0.1 percent.

Next, the figure-eight support with two test devices was run as a torsion pendulum in order to determine the moment of inertia, I_s, of the system. Again equation (5) is used, but this time it is solved for I_s, using the known value of S for the fiber. The values obtained (using fiber No.2) for the pendulum with test devices No.1 and No.3 are:

	I_s
No.1 type devices	4.6416×10^{-4} kg-m^2
No.3 type devices	1.6871×10^{-3} kg-m^2

The symmetric test device, type No.2, was not calibrated (but could be) since its main use up to the present has been in evaluating features involving symmetry of the device support and electric wind.

Once these values of I_s are known, each pendulum with a particular type of device can be used to check the calibration of torsion fiber directly, without the need to reuse the calibration cylinder. This is particularly useful once the devices are closed in the test chamber and a vacuum is established. No great use of this feature has been made to date, but it allows recalibration to be carried out in a straight forward manner during a test series, if desired.

It should be noted that the moment of inertia I_s only needs to be known in order to recalibrate the fiber with the test device pendulum. The original fiber calibration value of S can be used to determine the force generated by any particular device set-up, provided the temperature or resulting axial tension does not otherwise alter the value of S. Therefore, the fact that the moment I_s was not determined for the No.2 type devices (symmetric

toroids) above, does not preclude determining force values from deflections observed during tests with this unit.

The force, F, on each test device is obtained directly using the following expressions:

$$\theta = (x - x_o)/2r \quad (7)$$

$$Q = S\theta \quad (8)$$

$$F = Q/2R \quad (9)$$

where

x_o= zero position on linear scale(no force applied)
x= final position on linear scale(after force applied)
r= mirror to scale distance
θ= angular deflection of mirror and devices, and angle of twist of the torsion fiber; radians
S= torsional stiffness; $N\text{-}m^2$
Q= total torque on fiber; N-m
R= moment arm of each device about fiber axis; m
F= force on each device; N.

These relations can, of course, be combined into a single expression for evaluating F. It has been used in reducing test data under this program.

Device Tests

The propulsion device tests conducted under the program fall with two major groups according to the asymmetrical or symmetrical nature of the device. Secondarily, tests were conducted with the test devices mounted to swing in the complete

chamber (a condition referred to "open chamber"), or to swing inside a stationary hollow conducting ball (a condition called "inside ball") The test devices were located at the same position with respect to the chamber in the two cases; the ball was simply mounted to surround the devices in the one case. As noted previously, the ball was introduced in order to measure diffusion current from the devices under test.

Initially several shakedown type tests were conducted in the open chamber at atmospheric pressure using a modified form of the asymmetrical test device No. 1. These tests were to examine the nature and behavior of the overall test configuration. The devices tested had a small dielectric ring placed around the edge of the plate to help prevent the edge region from becoming a source for electrical discharge. This ring had a cross-sectional diameter of about 0.00416 m (0.188 inch), centered at the edge of the disk. These tests indicated that even this small amount of dielectric caused inconsistencies in device performance, much as if the electrical characteristics of the dielectric changed successively during the first few tests. Whether this behavior would stabilize after many tests is unknown. As a result, the shakedown tests' results are greatly suspect and have been omitted from this report.

After shakedown, the dielectric rims were removed so the test devices reverted to the all metal ball and disk form of device No. 1.

Test conditions and resulting forces measured with asymmetrical devices numbers 1 and 3 are given in Table 7. The tests cover a range of pressures from atmospheric to 1.33 Pascal (10^{-2} torr). At atmospheric pressure, driving voltages from 0.5 to 6.04 kilovolts were used. Under partial vacuum conditions of 1.33×10^{3} Pascal (10 torr) or less, these applied voltages were generally limited to 0.5, 1.0 or 1.5 kilovolts. This was so the applied voltage would remain under a Paschen type voltage

breakdown curve, where the applied voltage would not cause arc or spark breakdown to occur. As the results in Table 7 indicate, arcing did occur occassionally anyway. It was especially difficult to obtain force measurements at pressures of 13.3 Pa (10^{-1} torr) and 133 Pa (1 torr), which lie in the region where the voltage breakdown is a minimum for the test configuration used. This minimum breakdown voltage was just above 500 volts. This pressure region, on the other hand, is most important in examining electrical wind which may be present.

It will be noted that Table 7 includes data for only one successful test (No. 42) with device No. 3, which included the truncated dielectric cone. Several abortive attempts were made to conduct further tests with this device, but after the first run the dielectric had changed, and it continued to change. The total force became less and less with successive runs, until essentially no deflections were observed.

The final group of tests, numbers 43 through 50, in Table 7 were run under the open chamber condition. The results of these tests were compared with those made earlier inside the sphere to determine whether the sphere boundary affected the total force measurements. This comparison indicated that the influence of the boundary on the total force measurement is not appreciably different whether the sphere is present or absent, at least for the relatively low voltage test conditions used. This finding will need further verification for conditions of higher driving voltages.

Measured values of the average total force acting on the asymmetrical test device No. 1 are presented in Figure 6 as a function of vacuum level, with the voltage applied across the device as a parameter. The number alongside each point designates the corresponding test number from which the data for the point originated.

TABLE 7. ASYMMETRICAL DEVICES TEST DATA SUMMARY

Test No.	Date-Time Mo-Da-Hour	Device No.	Pressure Pa(torr)	Voltage* (volts)	Temperature $^{o}C(^{o}F)$	Deflection** (inches)	Total Force Newton	Remarks
1-8A	12-8,9-	1						Shakedown Tests
				(INSIDE 16" FIXED BALL)				
9	12-14-1000	1	$1.33(10^{-2})$	575	13.1(55.6)	-0.065	$-2.502x10^{-8}$	2nd Fiber
10	12-14-1024	2	$1.33(10^{-2})$	575	13.1(55.6)			No Motion (stuck in Hg-S/Hg)
11	12-14-1031	1	$1.33(10^{-2})$	1060	13.1(55.6)			No Motion. S/Hg
12	12-14-1104	1	$1.33(10^{-2})$	2000	14.0(57.2)			Zero changed during run
13	12-14-1150	1	$1.33(10^{-2})$	3000	14.9(58.8)			No Motion. S/Hg
14	12-15-1408	1	$1.01x10^{5}(760)$	550	16.1(61.0)			No Motion. S/Hg
15	12-15-1425	1	$1.01x10^{5}(760)$	1480	16.5(61.7)	+.210	$+8,084x10^{-8}$	
16	12-15-1508	1	$1.01x10^{5}(760)$	3000	16.6(61.8)	+1.100	$+42.34x10^{-8}$	
17	12-16-1529	1	$1.01x10^{5}(760)$	4500	16.6(61.8)	+1.9925	$+76.70x10^{-8}$	
18	12-16-0850	1	$1.01x10^{5}(760)$	6040	13.3(56.0)	+4.625	$+178.04x10^{-8}$	
19	12-16-1106	1	$1.33x10^{3}(10)$	560	14.7(58.4)			No Motion. S/Hg
20	12-16-1113	1	$1.33x10^{3}(10)$	1020	14.8(58.6)			No Motion. S/Hg
21	12-16-1136	1	$1.33x10^{3}(10)$	1500	15.1(59.2)	-0.0875	$-3.368x10^{-8}$	
22	12-16-1202	1	$1.33x10^{3}(10)$	3000	15.4(59.3)			ARC

TABLE 7. ASYMMETRICAL DEVICES TEST DATA SUMMARY (cont.)

Test No.	Date-Time Mo-Da-Hour	Device No.	Pressure Pa(torr)	Voltage* (volts)	Temperature °C(°F)	Deflection** (inches)	Total Force Newton	Remarks
23	12-16-1206	1	$1.33x10^{3}$(10)	2500	15.4(59.8)			ARC
24	12-16-1210	1	$1.33x10^{3}$(10)	2000				ARC
25	12-16-1405	1	2.66($2x10^{-2}$)	1000	16.1(61.0)			Zero changed during run
26	12-16-1424	1	2.66($2x10^{-2}$)	1000	16.4(61.6)			Lost electrical contact.
27	12-16-1503	1	2.66($2x10^{-2}$)	1500	16.9(62.4)	-.115	$-4.427x10^{-8}$	
28	12-16-1600	1	2.66($2x10^{-2}$)	1500	17.3(63.2)	-.110	$-4.234x10^{-8}$	
29	12-17-0912	1	1.33(10^{-2})	1500	17.0(62.6)	-.150	$-5.774x10^{-8}$	
30	12-17-0951	1	1.33(10^{-2})	1000	17.1(62.8)	-.080	$-3.080x10^{-8}$	
31	12-17-1025	1	1.33(10^{-2})	1500	17.4(63.4)			Zero changed. Test concluded early.
32	12-17-1044	1	1.33(10^{-2})	500	17.6(63.6)			No motion. S/Hg
33	12-17-1109	1	1.33(10^{-2})	5000	17.8(64.0)	-.3025	$-11.645x10^{-8}$	
34	12-17-1155	1	13.3(10^{-1})	500	17.8(64.0)	-.0675	$-2.598x10^{-8}$	
35	12-17-1315	1	$1.33x10^{3}$(10)	1000	17.6(63.7)			No motion. S/Hg
36	12-17-1330	1	$1.33x10^{3}$(10)	1000	17.7(63.8)			Lost electrical contact
37	12-17-1405	1	$1.33x10^{3}$(10)	1000	17.9(64.2)			Zero reference lost

TABLE 7. ASYMMETRICAL DEVICES TEST DATA SUMMARY (cont.)

Test No.	Date-Time Mo-Da-Hour	Device No.	Pressure Pa(torr)	Voltage* (volts)	Temperature $^{o}C(^{o}F)$	Deflection** (inches)	Total Force Newton	Remarks
38	12-18-0819	1	$1.01x10^{5}(760)$	1500	15.0(59.0)			No motion. S/Hg
39	12-18-0842	1	$1.01x10^{5}(760)$	1500	15.3(59.6)	+.455	$+17.516x10^{-8}$	
40	12-18-0908	1	$1.01x10^{5}(760)$	1000	15.4(59.8)	+.100	$+3.850x10^{-8}$	
41	12-18-0922	1	$1.01x10^{5}(760)$	500	15.7(60.2)	+.0425	$+1.636x10^{-8}$	
42	12-28-1538	3	$1.01x10^{5}(760)$	500	16.7(62.0)	+.0700	$+2.695x10^{-8}$	Dielectric inside ball.
					(OPEN CHAMBER)			
43	1-15-0954	1	$9.31x10^{2}(7)$	1000	12.0(53.6)			Zero reference lost.
44	1-15-1030	1	$9.31x10^{2}(7)$	1500	12.2(54.0)			ARC
45	1-15-1045	1	$1.33x10^{3}(10)$	1500	12.9(55.2)			ARC
46	1-15-1053	1	$1.33x10^{3}(10)$	500	13.0(55.4)	-.148	$-5.697x10^{-8}$	Zero shift.
47	1-15-1343	1	$1.33x10^{2}(1)$	500	13.0(55.4)	-.052	$-2.002x10^{-8}$	
48	1-15-1412	1	$13.3(10^{-1})$	500	14.0(57.2)			ARC

TABLE 7. ASYMMETRICAL DEVICES TEST DATA SUMMARY (cont.)

Test No.	Date-Time Mo-Da-Hour	Device No.	Pressure Pa(torr)	Voltage* (volts)	Temperature $^{o}C(^{o}F)$	Deflection** (inches)	Total Force Newton	Remarks
49	1-15-1455	1	$2.66(2x10^{-2})$	1000	14.8(56.6)			ARC
50	1-15-1504	1	$2.66(2x10^{-2})$	500	14.8(58.6)	-.048	$-1.848x10^{-8}$	

*Potential of the disk of test device No. 1 is positive with respect to the ball. The ball is at the same earth ground potential as the chamber.

**The direction of motion is indicated as positive when the device moves in the sense from the ball to the plate.

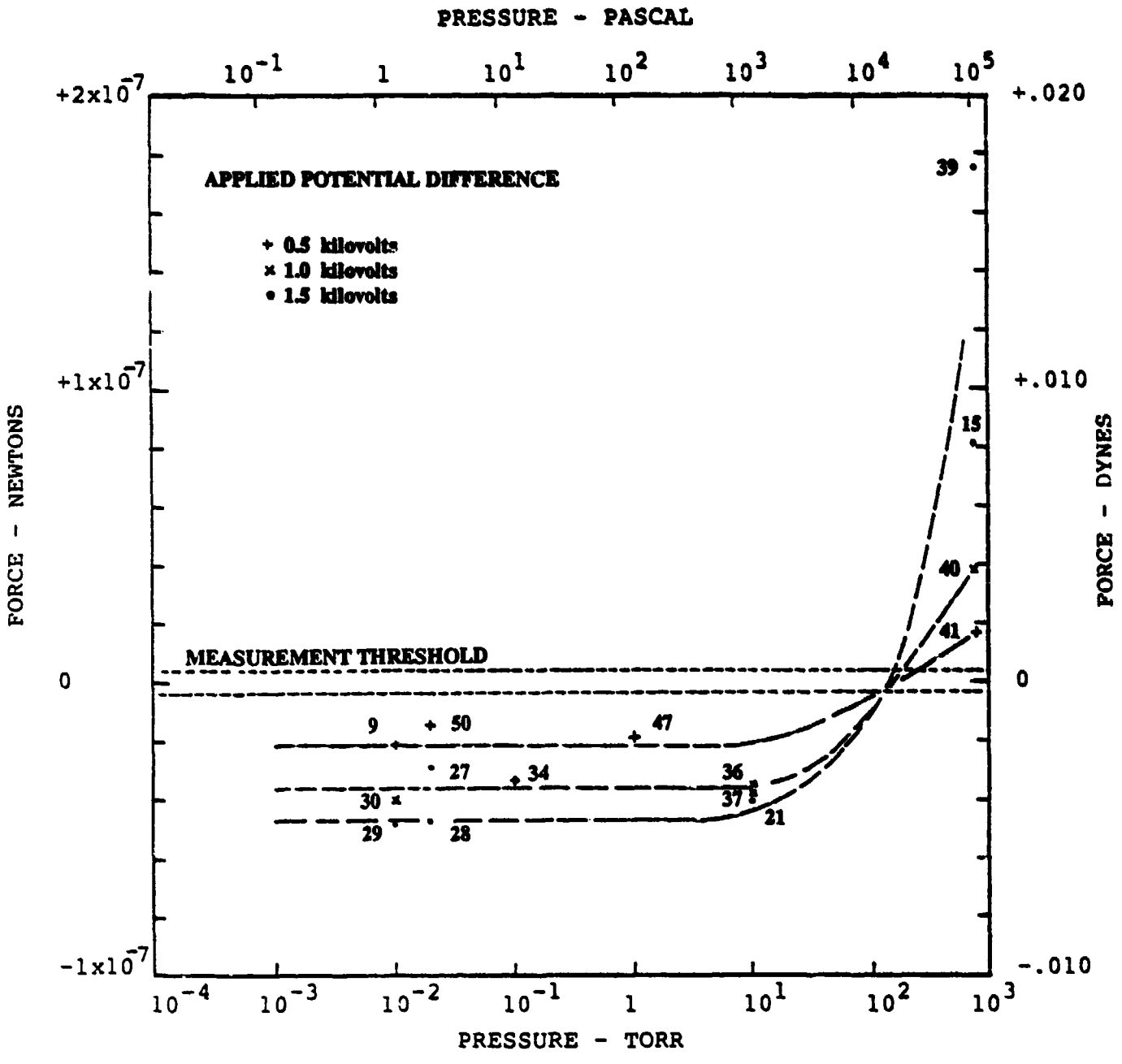

Figure 6. Variation of Measured Force With Air Pressure

The positive direction of force indicated in Figure 6 is from the ball towards the disk for device No. 1. For the test results shown, the disk was always at a positive potential with respect to the ball, and the ball was at the same earth ground as the chamber walls. The stationary hollow aluminum sphere placed around the test device support was held at earth ground potential when leakage currents were not being measured. It was connected through a 10k ohm resistor to ground during current measurements. Since the observed leakage currents were less that about 1 nA, the potential of the sphere was essentially zero also.

The region on Figure 6 labelled "measurement threshold" is bounded by the approximate positive and negative force levels that correspond to the combined effect of oscillation "noise" in the torsion pendulum and readout uncertainties. Forces measured with the current torsion fiber system are not reliable when their absolute values lie within this threshold region. In this region the forces are considered to be approximately zero.

The average force values given in Figure 6 include the contribution of the electrical wind, the ion propulsion effect, and presumably the Brown effect. It appears that the electrical wind force is appreciable at and near atmospheric pressure, but falls off to zero by the time the pressure is reduced to about 133 Pa (1 Torr). This pressure limit may be slightly lower for higher applied potentials. This behavior needs to be explored further in future investigations. The electric wind region indicated, however, is consistent with investigations noted in the literature;[16]-[19] apparently this phenomenon has received little attention in regions of higher vacuum.

The net force on the device in the region where electrical wind predominates is in the direction toward the more positive potential, as indicated by Brown. In the vacuum region, however, our measurements show this force to be in the opposite direction. Brown claimed (as noted in the "Background and Review of Selected

Observations") that under vacuum conditions the force was "in the negative to positive direction."[4] This discrepancy in the direction of force has not yet been resolved. If our results remain valid when further tests and other possible minor effects are taken into account, then it seems that the force measured here is not the same one Brown claimed to have investigated.

In the pressure region below about 133 Pa (1 Torr) the total force level associated with each potential appears to be independent of pressure. Further, the lack of significant boundary influence in tests run inside and outside the current collecting sphere is apparent. Test numbers 47 and 50 were run with no sphere present, whereas test numbers 9 and 34 were run with devices mounted inside the sphere.

The pressure independence also implies that any specific force level should exist unchanged even at atmospheric pressure, and should add (algebraically) to the electric wind force to give the total force actually measured. Near atmospheric pressure the electric wind force, in turn, would be larger than the total measured force shown in Figure 6.

The variation of total force with applied potential difference is shown in Figure 7 for forces on test device No. 1 at atmospheric pressure. The line through the data points is a regression line fitted to the points. On a logarithmic basis the equation of this line is

$$\log F = a + b \log V, \tag{10}$$

or in terms of physical parameters, it corresponds to the simple functional form

$$F = A V^b, \tag{11}$$

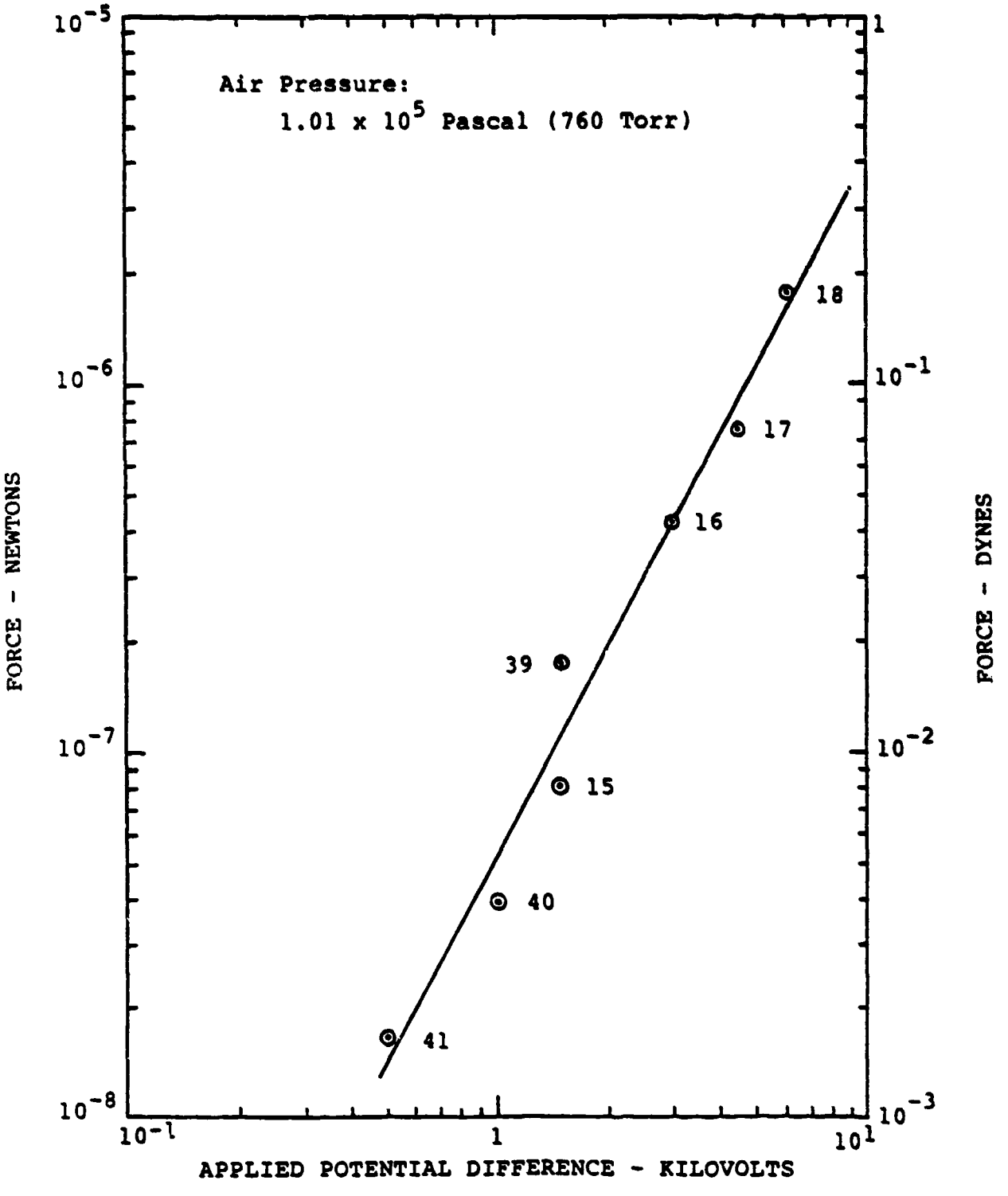

Figure 7. Variation of Measured Force With Applied Potential Difference

where

F= measured force

V= applied potential difference

A= constant = 10^a

b= line slope (on log-log plot).

For the data of Figure 6, the regression line becomes approximately

$$F = 5.21 \times 10^{-8} V^{1.888}, \quad (12)$$

where F is expressed in newtons and V is in kilovolts.

Forces in the pressure region at and below 1.33 Pa (1 Torr), which do not seem to vary with pressure, are combined at selected levels of applied voltage and are plotted in Figure 8. Error bars about the mean value points at 0.5 and 1.5 kilovolts represent the positive and negative values of one standard deviation estimated from experimental data. These values correspond to $\pm$ 20.6 percent and $\pm$ 17.4 percent of the means, respectively. Corresponding error estimates for the single points at 0.575, 1.0 and 5.0 kilovolts are each assumed to be $\pm$ 21% of the respective measured force values.

The regression line in this case becomes

$$F = 3.55 \times 10^{-8} V^{0.722}, \quad (13)$$

using the same units as before.

The exponents in each of the preceding functional forms are rather sensitive to the actual data, and hence, to any minor systematic errors in the measured values. The values given, therefore, should be considered preliminary.

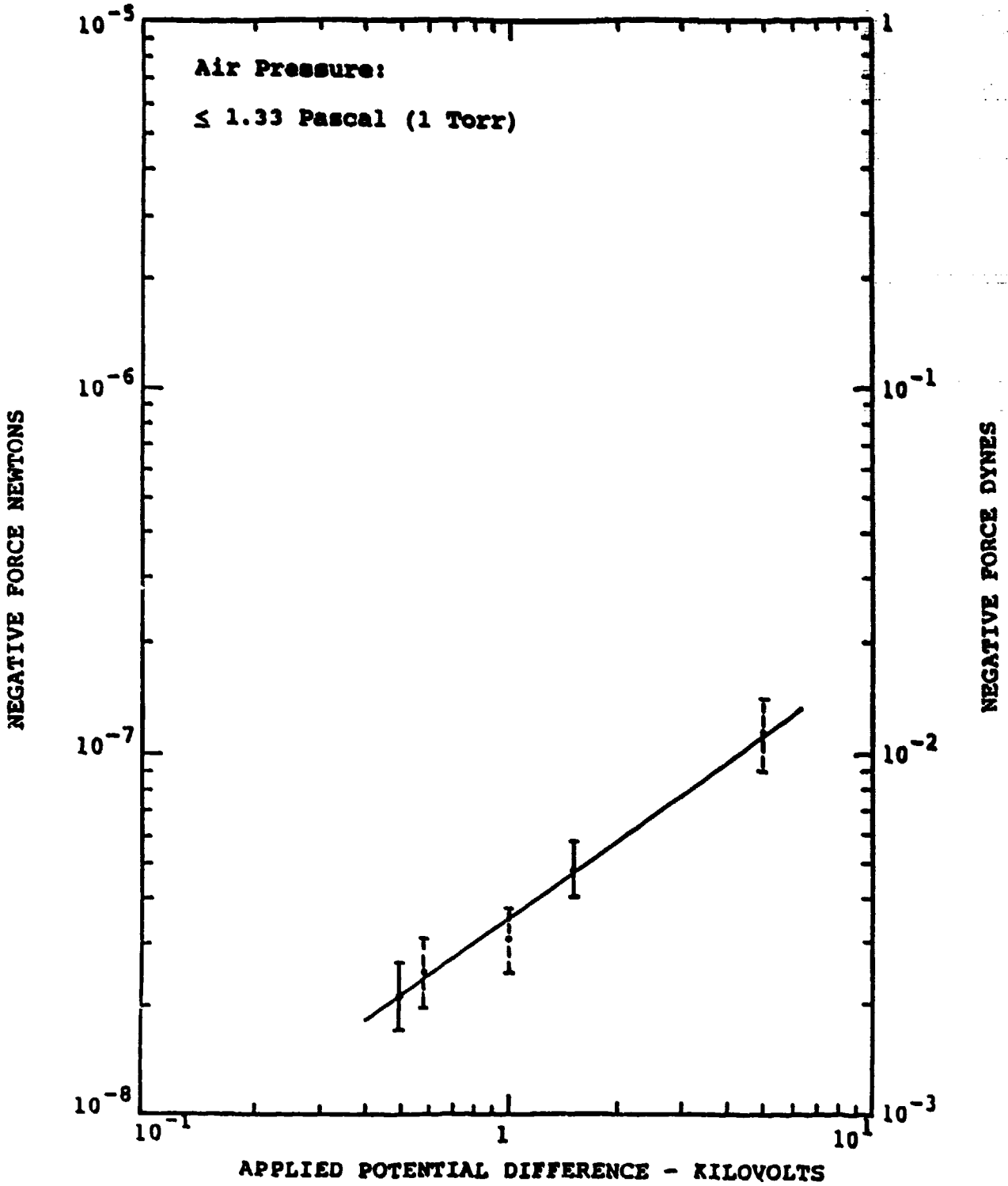

Figure 8. Variation of Measured Force With Applied Potential Difference

Results for tests conducted inside the hollow sphere using the symmetrical device No.2 are given in Table 8. The purpose of these tests was to determine if the figure-eight device support produced an asymmetrical force, and whether such a force, if present, was due to electrical wind. In view of Brown's work, the symmetrical device, itself, should produce no net force due to either the electrical wind or to the Brown effect. These tests were conducted using different combinations of electrical potentials on the two toroids and different grounding arrangements. The electrical conditions for each test run are shown in Table 9.

For all cases the electrical connections between the terminals at the bottom of the figure-eight support (or equally at the top of the stand pipe) and the device elements remains fixed. The center terminal indicated in Figure 9, is always connected to the ball end of the asymmetrical device, or to the toroids of the symmetrical device which fastens onto the same support arm. Likewise, the outside terminal fastens to the disk of the asymmetrical device, or the other toroid in the symmetrical case.

r reference, all the tests noted previously for asymmetrical devices were run using electrical condi' 'n #1, given in Table 9.

There is a slight asymmetry in the figure-eight device support shown earlier in Figure 4, consisting of the mechanical support ring for the brass tubes that hold the disks of the asymmetrical device. This same ring also serves as an electrical connection between the two disks and the vertical brass tube which ultimately connects to the outside terminal at the top of the stand pipe, as shown in Figure 5.

TABLE 8. SYMMETRIC DEVICE DATA SUMMARY

Test No.	Date-Time Mo-Da-Hour	Device No.	Pressure Pa(Torr)	Voltage (volts)	Temperature $^{o}C(^{o}F)$	Deflection (inches)	Total Force (Newton)	Remarks
1T	12-30-1044	2	$1.01x10^{5}$(760)	1500	16.4(61.6)	+.0225	$+ .866x10^{-8}$	
2T	12-30-1057	2	$1.01x10^{5}$(760)	1500	16.3(61.4)	+.095	$+3.657x10^{-8}$	
3T	12-30-1323	2	$1.01x10^{5}$(760)	1500	16.1(61.0)	+.0875	$+3.368x10^{-8}$	
4T	12-30-1343	2	$1.01x10^{5}$(760)	1500	16.1(61.0)			No motion.
5T	12-30-1403	2	$1.01x10^{5}$(760)	1500	16.4(61.6)	-.010	$- .385x10^{-8}$	Noise deflection.
6T	12-30-1418	2	$1.01x10^{5}$(760)	1500	16.6(61.8)	+.135	$+5.197x10^{-8}$	
7T	12-31-1044	2	$1.01x10^{5}$(760)	1000	15.6(6.0)	+.1075	$+4.138x10^{-3}$	
8T	12-31-1111	2	$1.01x10^{5}$(760)	500	15.3(59.6)	-.0275	$-1.059x10^{-8}$	
9T	12-31-1132	2	$1.01x10^{5}$(760)	1000	15.8(60.2)	+.010	$+ .385x10^{-8}$	Noise deflection.
10T	12-31-1510	2	$1.19x10^{3}$(9)	1000	16.1(61.0)	+.015	$+ .577x10^{-8}$	Noise deflection.
11T	12-31-1528	2	$1.19x10^{3}$(9)	1000	16.1(61.0)	-.0125	$- .481x10^{-8}$	Noise deflection.
12T	12-31-1551	2	$1.19x10^{3}$(9)	1000	16.1(61.0)	+.0075	$+ .289x10^{-8}$	Noise deflection.
13T	NO TEST							
14T	12-31-1615	2	$1.19x10^{3}$(9)	1000	16.1(61.0)	+.0075	$+.289x10^{-8}$	Noise deflection.

Table 9. Electrical Conditions for Symmetrical Device Tests
Signs of Electrical Potentials on Terminals at Top of Standpipe

CONDITION	CENTER TERMINAL	OUTSIDE TERMINAL	GROUND TERMINAL
# 1	-	+	Center (-)
# 2	+	-	Center (+)
# 3	+	-	Outside (-)
# 4	-	+	Outside (+)

TEST NO. (TABLE 8)	ELECTRICAL CONDITION #	TEST NO. (TABLE 8)	ELECTRICAL CONDITION #
1 T	1	8 T	4
2 T	3	9 T	2
3 T	3	10 T	2
4 T	1	11 T	4
5 T	2	12 T	1
6 T	4	13 T	-
7 T	4	14 T	3

It is perhaps easiest to grasp the symmetry test results by examining Table 10, where the measured total force values are indicated, together with test run number, in an array corresponding to given electrical conditions and potential differences applied to the device.

First, it is noted that the measurement threshold corresponds to a force of about $.385 \times 10^{-8}$ newton. Hence, the force values under condition #2 at atmospheric pressure are essentially zero. The values for conditions #1 and #4 combine to

Table 10. Array for Comparison of Forces Measured Using Symmetrical Device

Entry: Measured force, newtons(symmetrical device test number)

ELECTRICAL CONDITION	APPLIED POTENTIAL DIFFERENCE		
	1500 VOLTS	1000 VOLTS	500 VOLTS
Pressure: 1.01×10^{5} Pa(760 torr)			
# 1	$-.866 \times 10^{-8}$(1T)	----	----
# 2	$-.385 \times 10^{-8}$(5T)	$+.385 \times 10^{-8}$(9T)	----
# 3	$+3.657 \times 10^{-8}$(2T) $+3.368 \times 10^{-8}$(3T)	----	----
# 4	$+5.197 \times 10^{-8}$(6T)	$+4.138 \times 10^{-8}$(7T)	1.059×10^{-8}(8T)
Pressure: 1.19×10^{3} Pa(9 torr)			
# 1	----	$+.289 \times 10^{-8}$(12T)	----
# 2	----	$+.577 \times 10^{-8}$(10T)	----
# 3	----	$+.289 \times 10^{-8}$(14T)	----
# 4	----	$-.481 \times 10^{-8}$(11T)	----

indicate a bias in the force of approximately $+2.1 \times 10^{-8}$ newton. This corresponds to the polarity used in the asymmetric tests. The bias causes the force measured under the #1 condition to be more positive (less negative) than would be the case without the bias. This bias is attributed to the figure-eight device support hardware (probably associated with the asymmetrical support ring mentioned above), since the toroids of the No.3 devices used are quite symmetric and their force contribution should be zero.

A similar bias, with the same sign but with smaller magnitude (about $+1.6 \times 10^{-8}$ newton) also exists for the electrical conditions #2 and #3. In this case the electrical polarity at the device terminals are reversed.

The most important feature, however, is that at the pressure of 1.19×10^{3} Pa(9 torr), each of the forces measured at atmospheric pressure has essentially disappeared. The force values for conditions #2 and #4 which are slightly in excess of the measurement threshold, are still considered to be a noise deflection. This disappearance of measured forces implies that the forces observed with the symmetrical devices at atmospheric pressure are caused by electrical wind. In turn, this source of wind interaction is most likely the figure-eight support, and particularly the metal ring. This slight asymmetry does not seem to be operative at reduced pressures, so the previous test results with the asymmetrical test devices should be unaffected.

Auxiliary Tests and Considerations

A few auxiliary tests were conducted in attempt to further define or estimate the importance of factors which could influence the results obtained during tests of asymmetrical device No.1.

Perhaps the most important of the auxiliary tests were the ones run to assess the effect of lighting within the chamber on the torsion fiber, the test devices, and the residual air in the chamber.

Heating of the torsion fiber by incident radiation (especially under vacuum conditions) was examined briefly via comparison runs for a normal device load with the fiber shielded, with the radiation turned off, and with radiation turned on as used during device test runs. These several conditions appeared to have no effect on fiber performance or drift when they were

individually applied, or juxtaposed, over a period of about 30 minutes.

Direct application of radiation to the test devices in the open chamber indicated no measurable effects of radiation pressure. Inasmuch as the devices were inside the sphere during many of the test runs, radiation pressure effects were not expected to be influential during those particular test runs.

Radiant heating of air (or gas) in the chamber does cause mild convection currents to appear when the air pressure is near atmospheric. At reduced pressured of about 1.33×10^3 Pa(10 torr) or less no convection currents strong enough to influence force readings were observed.

Magnetic effects were considered, but were essentially negated by the symmetrical design of the figure-eight device support and the current carrying electrical connections and cables.

The figure-eight support design was chosen and implemented for two reasons; first, to eliminate the need to place a specific dielectric material between the electrodes of the test devices; and second, to balance any residual electric wind forces between support arms so that no net torque would act on the fiber.

Other auxiliary considerations, such as boundary effects, electrical breakdown conditions, use of symmetrical devices, changing electrical polarities, and use of different grounding points have been noted previously and are relevant.

System Errors

Any measurement system is subject to errors, both random and systematic, and the torsion fiber system used in this effort was no exception.

The principal random errors encountered were a slow zero drift of the fiber and a fast shift of the apparent zero position of the fiber, usually when an electrical potential was applied to the devices under test. The slow zero drift was straight forward to assess, since the zero positions were evaluated both before and after each test run. The fast shift proved more difficult, and was apparently not directly associated with the fiber behavior, but with that of the mercury when an electrical potential was applied. This can likely be circumvented by eliminating the mercury contacts from the system.

The main sytematic error encountered was the mechanical drag of the mercury on the electrical contacts mounted to the oscillating device pendulum. This drag tended to reduce the deflection of an electrically driven device, thereby indicating that a smaller total force was causing the device to deflect. This is another key reason for eliminating the use of mercury for electrical contacts.

A second systematic error is unconfirmed, but is apt to be associated with a changing value of the torsional stiffness, S, of the copper fiber used, with temperature and with applied load on the fiber. Copper is probably not strong enough or sufficiently stable to serve as a trouble free fiber for this application; tungsten is believed to be a better choice.

Evaluation

The total force measurements need to be compared to estimates of the magnitudes of the electric wind and ion propulsion effect to determine if any residual force exists.

In this program, asymmetrical devices were used for testing purposes to emphasize the Brown effect rather than electric wind. Given this selection, the burden of accounting for the magnitude

of the electric wind during this effort was placed on measurements of the total forces generated electrostatically rather than on calculated results. The geometry of the asymmetric ball and disk are such that direct calculation of the electric wind effect for this type of device becomes a significant three-dimensional axisymmetric boundary value problem. The major difficulty arises because the electric field and induced air flow (electric wind) are coupled and are generally not in the same direction at any point in the longitudinal plane, which includes the symmetry axis of the device. While such calculations can be made, they were not considered to be within the scope of the Phase I effort.

It is of interest to note, however, that an analytical model has been advanced by Cheng[20] for a simple one-dimensional case of electric wind generation by a device consisting of closely spaced parallel planar electrodes constructed of light wire meshes. When these electrodes are driven with a DC potential difference of several kilovolts, a thrust is generated that consists of electric pressure and electric wind. The electric pressure arises from a nonuniform electric field energy density between the electrodes (the nonuniformity results from space charge effects); the electric wind arises from the induced flow of neutral air molecules. For the sake of simplicity, the energy density term has not been separately called out in this report; instead, it has been included as part of the electric wind effect itself. Both electric pressure and electric wind cause a force on the device described by Cheng, which acts in a direction towards the positive electrode, just as observed here and as observed by Brown.

It is considered desirable in any follow-on effort to incorporate a device configuration that will allow direct comparison of test results with Cheng's model. This should help corroborate experimental findings with theory and strengthen the interpretation of any residual force effects observed.

The magnitude of the ion propulsion effect depends on the size of the diffusion current not collected by the disk or ball of the asymmetrical device No.1, but which passes to and is collected by the conducting sphere surrounding the test devices. The limit of sensitivity of the metering system used to evaluate the leakage current to the sphere was 1 nA. At no time (except during electrical breakdown) during the test runs under a vacuum was a measurable value observed in excess of this current sensitivity limit. Thus 1×10^{-9} ampere represents an upper bound on the current expected to contribute to the ion propulsion effect.

A general expression for the force, F, expected from such an electrostatic thruster is given by Sutton and Ross [21]:

$$F = I\sqrt{\frac{2V\mu}{e}} \quad , \tag{14}$$

where

F= accelerating force, newton
I= propelling current flow, coulomb/sec
V= accelerating potential difference, volts
μ= mass of accelerated particle, kg
e= charge per particle, coulomb.

For a threshold current of $I= 10^{-9}$ amp, V= 1000 volts and $e= 1.60 \times 10^{-19}$ coulomb, equation (14) gives

$$F= 111.8\sqrt{\mu} \text{ newtons.}$$

If the accelerated particles were all electrons, protons, or aluminum ions (single charge) the corresponding maximum forces would be:

electrons: $\mu = 9.11 \times 10^{-31}$ kg

$F = 1.07 \times 10^{-13}$ newton = 1.07×10^{-8} dyne

protons: $\mu = 1.672 \times 10^{-27}$ kg

$F = 4.57 \times 10^{-12}$ newton = 4.57×10^{-7} dyne

aluminum ions: $\mu = 26.98 \times 1.66 \times 10^{-27}$ kg/AMU = 44.8×10^{-27} kg

$F = 2.37 \times 10^{-11}$ newton = 2.37×10^{-6} dyne.

The force per device would be one-half of each of these values.

These estimates assume that all the ion current would act collectively to propel each device in one direction. These force values per device are at most less than 1/1000 of the force measurement threshold value of $.385 \times 10^{-8}$ newton (0.000385 dyne).

Here these estimates for ion propulsion effects are negligible, and the extrapolation procedure suggested earlier is unneccessary. The measured total force values for pressures less than about 133 Pa (1 torr), as shown in Figure 6, are the forces sought.

These electrostatically generated interaction forces are in the opposite direction of the forces claimed to have been measured by T.T. Brown. Hence, these interaction forces will not be referred to as due to the Brown effect, but will be called residual forces.

CONCLUSIONS

The following conclusions have been reached based on the investigations of the Biefield-Brown effect conducted on this project:

1. Direct experimental results show that when an electrostatic potential difference is applied between asymmetrical electrodes of an all metal test device, a propulsive force is generated and it acts on this device.

2. This electrostatically induced propulsive force consists of at least three components: electrical wind, ion propulsion, and a significant residual force.

   a.The electrical wind acts in the direction from the negative to the positive electrode and occurs only for air pressures greater than about 133 Pascal (1 torr), at least for applied potentials in the low kilovolt range.

   b.The ion propulsion effect (estimated on a theoretical basis) is completely negligible for the tests conducted.

   c.The residual force acts (for the tests conducted and the test device used) in the direction from the positive to the negative electrode, i.e., opposite to the direction of the electrical wind force. This residual force was observed directly and remained independent of the partial vacuum level over the approximate range of 133 Pascal (1 torr) to 1.33 Pascal (10^{-2} torr). Observations further indicate that this residual force remained constant up to atmospheric

pressure and subtracted from the electrical wind to yield the total force actually measured.

3. The electrostatically generated residual forces measured here act in the opposite direction to the forces claimed to have been measured in a vacuum by T.T. Brown. As a result these forces are referred to as residual forces, and not as forces caused by the Brown effect.

4. The residual force appears to vary approximately as the 0.72 power of the potential difference applied to the asymmetrical propulsion device tested. This finding is based on only a few datapoints, and may need revision when more data become available.

5. The measured total force at atmospheric pressure, due to contributions from electrical wind and (presumably) the residual force, varies approximately as the 1.9 power of the potential difference applied to the asymmetrical propulsion device tested.

6. The magnitude of the residual force appears to be rather small, but the size, shape and configuration of the device tested are not necessarily optimal for residual force generation, and it may be possible to generate larger forces with devices similar in overall size.

7. Only cursory attention was given to the exploration of electrostatically induced propulsive forces using devices which incorporate dielectrics in their design. The few tests which were conducted at atmospheric pressure using such devices, exhibited problems with reproducibility.

8. The torsion fiber type measurement system employed in this program needs a few modifications to improve performance, but the overall measurement scheme appears suitable for investigating the fundamental aspects of electrostatically induced propulsive forces.

RECOMMENDATIONS

As a result of this investigation, it is recommended that measurements of propulsive forces generated on test devices by application of applied electrostatic potentials or fields be continued. The purpose of this activity would be to further verify the existence of the residual force noted in this report, and to develop a more extensive data base which can be used to more thoroughly explore and characterize its nature. Particular attention needs to be given to extending the range of test conditions to greater vacuum levels and to higher applied electrostatic potentials. Selected improvements in the overall measurement and test configuration need to be incorporated to facilitate test reproduciblity, more efficient data collection, and improved accuracy of measurements.

REFERENCES

1. G. Burridge, Townsend Brown and His Anti-Gravity Discs, Fate pp 40-46, 1956.

2. Rho Sigma, Ether Technology: A Rational Approach to Gravity-Control, Private Publication, Clayton, GA 1977, pp. 27-28, 39, 44-49.

3. T.T. Brown, "A Method of and an Apparatus or Machine For Producing Force or Motion," British Patent #300, 311, Nov. 15, 1928. p. 4, line 46.

4. T.T. Brown, Electrokinetic Apparatus, U.S. Patent 3,187,206, June 1, 1965.

5. T.T. Brown, How I Control Gravitation, Science and Invention. August 1929, p. 374.

6. Office of Naval Research, The Townsend Brown Electro-Gravity Device: A Comprehensive Evaluation by the Office of Naval Research, with Accompanying Documents, W.M. Moore Publications, Prescott, Az. Sept. 15, 1952.

7. L.B. Loeb, Electrical Coronas, University of California Press, Berkeley, 1965, pp. 402-406.

8. D.E. Gray (ed.) American Institute of Physics Hardbook, McGraw-Hill Book Co., New York, 1957, pp. 2-61, 3-78- 3-80.

9. A. Elliott and J.M. Dickson, Laboratory Instruments: Their Design and Application, Chemical Publishing Co., New York, 1960.

10. P.J. Geary, Torsion Devices, British Scientific Instrument Research Association Report R249, 1960.

11. C. Limb, Sur la determination du moment du couple de torsion d'une suspension unifilaire, Compte Rendus Vol. 114, pp. 1057-1060, May 9, 1892.

12. R.C. Weast (ed.), CRC Handbook of Chemistry and Physics, 55th Edition, CRC Press, Cleveland, 1975.

13. H.A. Pohl, Dielectrophoresis, Cambridge University Press, New York, 1978.

14. A.D. Moore, Electrostatics and Its Applications, John Wiley & Sons, Inc., New York 1973.

15. W.J. McGregor Tegart, Elements of Mechanical Metallurgy, MacMillan Co., New York, 1966, p. 97.

REFERENCES (CONT)

16. A.P. Chattock, Philosophical Magazine, Vol.48, p 401, 1899.

17. A.P. Chattock, Philosophical Magazine, Vol.1, p 79, 1901.

18. A.P. Chattock and A.M. Tyndall, Philosophical Magazine, Vol .17, p 543, 1909.

19. S. Rattner, Philosophical Magazine, Vol. 32, p 442, 1916.

20. S.I. Cheng, Glow Discharge as an Advanced Propulsion Device, ARS Journal Vol. 32, No. 12, pp 1910-1916, December 1962.

21. G.P. Sutton and D.M. Ross, Rocket Propulsion Elements, 4th ed., John Wiley and Sons, New York, 1976, p 481.

BIBLIOGRAPHY

AIAA Subcommittee 1971 "UFO Encounter I -- Sample case Selected by the UFO Subcommittee of the AIAA," Astronautics & Aeronautics. pp.66-70.

Bearden, T.E. and A. Michrowski, 1985 The Emerging Energy Science, Planetary Association for Clean Energy Inc., Ottawa, CA

Brown, T.T., 1928 "A Method of and an Apparatus or Machine for Producing Force or Motion," British Patent #300,311. Nov. 15, 1928.

Brown, T.T., 1929 "How I Control Gravitation," Science and Invention. August. pp.312-313, 373-375.

Brown, T.T., 1934 "Electrostatic Motor," U.S. Patent #1,974,483. September 25, 1934.

Brown, T.T., 1956 "Electrical Self-Potential in Rocks," The Psychic Observer and Chimes. 37(1) Jan.-Mar. pp.48-53.

Brown, T.T., 1956 "Electrokinetic Apparatus," The Psychic Observer and Chimes. 37(1) Jan.-Mar. pp. 34-40.

Brown, T.T., 1956 "The Fluid Pump," The Psychic Observer and Chimes. 37(1) Jan.-Mar. pp.54-59.

Brown, T.T., 1956 "How I Control Gravitation," The Psychic Obsrver and Chimes. 37(1) Jan.-Mar. pp.14-19.

Brown, T.T., 1960 "Electrokinetic Apparatus," U.S. Patent #2,949,550. August 16, 1960.

Brown, T.T., 1962 "Electrokinetic Generator," U.S. Patent #3,022,430. February 20, 1962.

Brown, T.T., 1962 "Electrokinetic Transducer," U.S. Patent #3,018,394, January 23, 1962.

Brown, T.T., 1965 "Electric Generator," U.S. Patent #3,196,296. July 20, 1965.

Brown, T.T., 1965 "Electrokinetic Apparatus, U.S. "Patent #3,187,206. June 1, 1965.

Brown, T. T., 1973 "Research in Shackles," Information and Letter from Brown

Brown, T.T., 1986 "The Scientific Notebooks of T.T. Brown," William L. Moore Publications & Research. Vol.1., Vol. 2.

Burridge, Gaston, 1956 "Townsend Brown and His Anti-Gravity Discs," FATE, pp.40-46.

Chattock, A.P. 1899 Philosophical Magazine. Vol 48, p. 401.

Chattock, A.P. 1901 Philosophical Magazine. Vol 1, p. 79.

Chattock, A.P. and A.M. Tyndall 1909 Philosophical Magazine. Vol 17, p. 543.

Childress,D.H. 1985 The Anti-Gravity Handbook, Publishers Network/Adventurer Unlimited Press, Stelle, IL, 1985.

Christenson, Edward and Paul Moller 1967 "Ion-Neutral Propulsion in Atmospheric Media," AIAA Journal. Vol.5(10)., pp. 1768-1773.

Cleaver, A.V., 1957 "Electro-Gravitics: What it is--or Might Be," Journal of the British Interplanetary Society. Vol.16, pp.84-94.

Coll. Univ. Wisdom 1966 "The Biefield-Brown Effect," "Proceedings" College of Universal Wisdom, Yucca Valley, Calif., Volume 8, Aug.-Oct. pp. 1-4, 4-6, 36-41, 87.

DeSeversky,A.P. 1964 "Ionocraft," U.S. Patent #3,130,945, April 28, 1964.

Gravity Rand, Ltd. 1956 "The Gravitics Situation." pp.3-30.

Hagan, D.E. 1964 "Flying Apparatus," U.S. Patent #3,120,363. February 4, 1964.

Intel, 1956 "Towards Flight without Stress or Strain...or Weight," Inter Avia. Vol.11(5), pp.373-375.

Intel, 1956 "Towards Flight without Stress or Strain...or Weight," The Psychic Observer and Chimes. 37(1) Jan.-Mar. pp.10-13.

Mead, F.B.,Jr., and J. E. Cox 1976 "Laboratory of T. Townsend, Sunnyvale, CA," Trip Report, January 24 & 25.

Moore, W.L. 1979 "The Force Fields of Townsend Brown." The Philadelphia Experiment. Fawcett Crest Books: New York. pp.207-225.

Naval Research Off. 1952 "The Townsend Brown Electro-Gravity Device," A Comprehensive Evaluation by the Office of Naval Research, with Accompanying Documents. W.M. Moore Publications, Prescott, AZ, September. 15.

Rattner, S. 1916 Philosophical Magazine. Vol 32, p. 442.

Rose, Mason, 1956 "The Flying Saucer," The Psychic Observer and Chimes. 37(1) Jan.-Mar. pp.20-27.

Schaffranke, R 1975 "Letter to the Editor--Energy Research: is America Losing the Ball?" Astronautics & Aeronautics. Vol.37(1). pp.46-47, 69.

Sigma Rho 1972 Forschung in Fesseln, Ventla-Verlag, Originalausgabe 1972, VENTLA-Verlag, D-6200 Wiesbaden-Schierstein

Sigma, Rho, 1972 "Research in Bondage, The Riddle of the Electro-Gravitation." pp. 11-22 (translation)

Sigma, Rho, 1977 Ether-Technology: A Rational Approach to Gravity-Control

Thomas, W.R. and J. L. Martin 1956 "Evaluation of T. Townsend Brown's Electrokinetic Apparatus," The Psychic Observer and Chimes, 37(1). Jan-Mar., pp. 42-45